Blue whiting in Icelandic waters: migration, residency, and population connectivity

Brendon Lee [1, 2, *] (0000-0003-1628-8905)

Anna H. Ólafsdóttir[2] (0000-0001-5048-2659)

Søren Post[3] (0000-0003-1091-9742)

Haseeb S. Randhawa[1, 4] (0000-0001-6262-970X)

[1] Faculty of Life and Environmental Sciences, University of Iceland, 101 Reykjavik, Iceland

[2] Marine and Freshwater Research Institute, 220 Hafnarfírði, Iceland

[3] Greenland Institute of Natural Resources, 3900 Nuuk, Greenland

[4] New Brunswick Museum, Saint John, New Brunswick, E2M 2K8 Canada

* Corresponding author: brendon@hi.is

Abstract

Widely distributed pelagic fish populations underpin some of the largest fisheries globally and play a critical role in ecosystem dynamics by driving nutrient cycling and carbon transfer through vertical and seasonal migrations. Effective fisheries management requires understanding their spatial distribution, abundance, size structure, and the environmental factors that drive temporal variations, especially in the context of climate change. Here, we investigate the population structure of blue whiting (*Micromesistius poutassou*) in Icelandic waters using Bayesian hierarchical

spatiotemporal models applied to bi-annual demersal survey data (1996–2023), which included 15,788 samples. Our results show that blue whiting occurrence, abundance, and size structure are influenced by physical (depth, bathymetric slope), environmental (SST, SBT), and temporal (time of day, year, season) factors. We identify three main spatial patterns: (1) persistent aggregations along the southern shelf and Iceland-Faroes Ridge, intensifying in spring; (2) marginal transition zones to the northwest and northeast with spatiotemporal variability; and (3) fringe subpopulations in the north. These findings suggest that migration from the dominant Northeast Atlantic population primarily drives autumn distributions, while partially resident juveniles persist in local nursery areas on the southern and western shelf year-round. This study provides vital knowledge for sustainable management on blue whiting stock level responses to future climate change.

Keywords: Distribution, abundance, population structure, *Micromesistius poutassou*, INLA, northeast Atlantic

1. Introduction

Marine fish populations exhibit significant variation in distribution, abundance, and demographic composition over time and space. Understanding these patterns can reveal population responses to environmental pressures and highlights spatial boundaries or structures among population units (Baudron et al. 2020, Cadrin et al. 2023). Such insights are crucial for understanding metapopulation dynamics and species biocomplexity (Smedbol & Stephenson 2001, Hilborn et al. 2003). In the northeast (NE) Atlantic, widely distributed pelagic fish, such as capelin (*Mallotus*

villosus), mackerel (*Scomber scombrus*), herring (*Clupea harengus*), and blue whiting (*Micromesistius poutassou*) occur in high abundance, possess extensive dispersal potential, and undertake large-scale migrations (Trenkel et al. 2014). These characteristics obscure complex population structures when viewed at broad regional scales, blurring distinctions among migratory and resident groups (Ciannelli et al. 2013). Recognizing and accounting for these complexities on both regional and local scales is thus crucial for building resilience against anthropogenic and environmental pressures, guiding sustainable fisheries management and informing effective conservation strategies (Kerr et al. 2017, Kearney & Hilborn 2022).

Blue whiting is an abundant, benthopelagic gadoid fish that is widely distributed across the north Atlantic and Mediterranean. In the NE Atlantic, they primarily inhabit depths of 200 to 600 m along the continental shelf-break and slope (Bailey 1982, Pointin & Payne 2014). Dominant spawning aggregations occur over the Porcupine Bank, the outer Hebrides, and Rockall Bank, west of the British Isles (Bailey 1982, Miesner & Payne 2018). They undertake extensive seasonal migrations into productive feeding areas, south along the European Shelf into the Bay of Biscay (Brophy & King 2007), northeast into the Norwegian Sea, and northwest of the Faroes, onto the Iceland and Greenland Shelves (Heino et al. 2008, Hátún et al. 2009a, Post et al. 2019). The northwestern branch of the distribution features dynamic environmental gradients and distinct oceanographic features, which could play a crucial role in shaping blue whiting population dynamics (Pampoulie et al. 2024). This region is shaped by the interaction between warmer northward-flowing Atlantic waters with colder Arctic inflows along the steep shelf-slope boundaries of the Greenland–Scotland Ridge (GSR) (Logemann et

al. 2013). Understanding these factors is essential for identifying species distribution, migration patterns and subpopulation structures in this area.

Blue whiting holds crucial ecological significance in the NE Atlantic ecosystem, serving as both predator and prey. They undertake diel vertical migrations, contributing to vertical energy transport in the water column (Johnsen & Godø 2007, Trenkel et al. 2014). They consume high-energy zooplankton and mesopelagic fish species, and provide sustenance for apex predators, including commercially valuable fish such as mackerel and cod (Gjøsæter et al. 2009, Dolgov et al. 2010, Pálsson & Bjarnasson 2011, Bachiller et al. 2016). Through their migratory and diel vertical movements, blue whiting connects temperate and polar ecosystems, and link surface production to the deep-sea (Trenkel et al. 2014). Economically, blue whiting supports large fisheries, with annual catches of 1.1 to 1.7 million tonnes since 2014 (ICES 2023).

Despite their ecological and economic importance, research has predominantly focused on the main spawning aggregation, and the population structure of blue whiting remains poorly understood. Studies on genetic variability (Giæver & Stien 1998, Ryan et al. 2005, Was et al. 2008), otolith shape (Keating et al. 2014, Mahe et al. 2016), otolith microstructure (Keating et al. 2014), egg and larval dispersal (Bartsch & Coombs 1997, Skogen et al. 1999), and spatial-temporal distribution of early life-history stages (Kloppmann et al. 2001, Pointin & Payne 2014) suggest a complex population structure with spatial and temporal variability. Evidence points to both a dominant migratory population, and localised resident subpopulations in areas like the Mediterranean, Romsdalsfjord (Norway), and the Barents Sea (Giæver & Stien 1998, Ryan et al. 2005). However, limited research exists on subpopulations in Icelandic

114 waters. Anecdotal evidence of recruitment in Icelandic and Greenland waters has
115 indicated the potential for a distinct population with a separate spawning source from
116 the main Hebrides-Norwegian stock (Sveinbjörnsson 1975, Post et al. 2019).
117
118 Research surveys monitoring abundance and distribution of fish stocks offer a
119 valuable opportunity to gather critical baseline information on the spatial patterns of
120 blue whiting in the region. The insights derived from these surveys can significantly
121 enhance our understanding of the species' population structure (Lindegren et al.
122 2022). This study focuses on investigating the population structure of blue whiting
123 around Iceland, with particular attention to how environmental factors shape their
124 occurrence, abundance, and size. We examine the spatial and temporal dynamics of
125 blue whiting populations while accounting for environmental variability, physical
126 factors, and seasonal and interannual variation. Our analysis aims to determine
127 whether these patterns indicate the presence of subpopulation structures. To achieve
128 this, the study is guided by four key objectives:
129
130 (1) Environmental and physical drivers: Identify the primary environmental factors
131 influencing blue whiting occurrence, abundance, and size structure in Icelandic
132 waters.
133 (2) Spatial persistence: Assess the consistency of blue whiting occurrence,
134 abundance, and size structure across different regions within Icelandic waters.
135 (3) Temporal dynamics: Analyse changes in occurrence, abundance, and size
136 structure of blue whiting populations over time.
137 (4) Population substructure: Integrate spatial and temporal findings to evaluate the
138 potential existence of distinct population substructures.

By highlighting the potential population substructures of blue whiting in Icelandic waters, this study aims to deepen our understanding of marine ecosystem dynamics and contribute to more effective fisheries management strategies. The findings will not only advance the scientific knowledge of blue whiting population dynamics but also provide crucial evidence to support policymakers in developing targeted conservation efforts, enhancing the resilience of the NE Atlantic ecosystem against climate change and other human-induced pressures.

2. Materials and Methods

2.1. Study Area

The study area encompasses the highly productive waters of the Iceland Shelf and slope, situated in the northeast Atlantic between 62-68°N and 8-30°W (Figure 1). The Iceland Shelf, ranging from 15 to 500 m in depth, extends 100 to 150 km from the coast of Iceland towards the west, north, and east, narrowing in the south where it deepens into the Iceland Basin (IB) (Astthorsson et al. 2007). A key topographical feature is the GSR, which forms a boundary between the southern/western and northern/eastern parts of the Iceland Shelf, providing a continuous link between the Greenland, Iceland, and European Shelves (Pampoulie et al. 2024). The southeast portion of the GSR, known as the Iceland-Faroe Ridge (IFR), connects the Iceland Shelf to the European Shelf. To the northwest, the Denmark Strait (DS) separates the broad western Icelandic shelf from the Greenland Shelf. In the south, the Reykjanes Ridge (RR), part of the Mid-Atlantic Ridge, forms the western boundary of the narrow

164 southern shelf as it broadens and deepens into the Irminger Sea. North of Iceland, the
165 Kolbeinsey Ridge (KR), a continuation of the Mid-Atlantic Ridge, extends through the
166 northern Icelandic waters, with the Iceland Sea to the NE.
167
168 These geological features shape oceanic circulation and water mass distribution
169 around the Iceland Shelf, leading to distinct oceanographic regions (Astthorsson et al.
170 2007, Logemann et al. 2013). The southern areas are influenced by the warm and
171 saline North Atlantic Drift (NAD) and the Irminger Current (IC), with temperatures
172 ranging from 6 to 11°C. In contrast, the northern regions are affected by the cold and
173 low saline waters of the southward-flowing East Greenland Current (EGC) and the
174 East Iceland Current (EIC), where temperatures range from below 0 to 2°C.
175 Additionally, a branch of the IC flows northward around the northwest peninsula,
176 impacting the northern Icelandic shelf and contributing to the distinct oceanographic
177 fronts found to the west and east of Iceland, where warm and cold waters converge.
178 Modelling studies provide further evidence of these complex circulation patterns,
179 highlighting their role in shaping the distribution of water masses and ecological zones
180 (Logemann et al. 2013). Mean annual primary production and zooplankton densities
181 are generally higher in the Atlantic water compared to the more variable waters north
182 of Iceland (Astthorsson et al. 2007).
183

184 **2.2. Survey Data**

185
186 Data on blue whiting occurrence, abundance, and length were collected during annual
187 groundfish surveys on the Icelandic continental shelf and slope, conducted by the
188 Marine and Freshwater Research Institute (MFRI) from 1996 to 2023. These surveys

189 took place in two seasons: Spring (late February to early April) and Autumn (mid-
190 September to early November). During the spring surveys, 509 to 596 stations were
191 sampled each year at depths ranging from 17 to 509 m (n = 15,788). Spring surveys
192 were originally designed for monitoring of shelf-based demersal fish species, such as
193 cod. In autumn, 290 to 400 stations were sampled annually at depths between 26 and
194 1452 m (n = 9,928). These surveys extended the distribution of the spring surveys into
195 slope-based waters for the monitoring of deep-water redfish populations. All surveys
196 employed a standardized research bottom trawl with a 40 mm stretched mesh size in
197 the cod end (Sólmundsson et al. 2020, Jónsdóttir et al. 2023a). The trawl net had
198 vertical and horizontal openings of 2–3 m and 17 m, respectively. Trawling was
199 conducted at a towing speed of 3.8 knots over four (spring) and three (autumn) nautical
200 miles. For each trawl station, the date, time, geographic coordinates (latitude and
201 longitude), and depths were recorded at both the start and end points. At each station,
202 the number of individual blue whiting was recorded, and fish were measured down to
203 the nearest centimetre. For trawl catches exceeding 100 individuals, a random
204 subsample was selected to measure length distributions at each station. The
205 subsample size was determined based on the observed length range, with at least two
206 individuals sampled for each centimetre of the length interval (e.g., a range of 5–30
207 cm yields a 25 cm interval, so 50 individuals are sampled). A minimum of 20 individuals
208 was used when the length range was narrow. This subsample was then extrapolated
209 to the total catch to estimate the numerical catch for each length class. To standardize
210 abundance estimates, abundance-at-length values were adjusted for differences in
211 the swept area, resulting in numerical catch-per-unit-effort (NPUE) data
212 (number.cm.tow^{-1}).
213

Although bottom trawl surveys are standardized, they are not specifically designed for benthopelagic species like blue whiting, potentially underestimating their true densities (Walker et al. 2017, Lindegren et al. 2022). However, the ICES working group for widely distributed stocks (WGWIDE) considers bottom trawl survey data reliable for assessing one-year old fish abundance (ICES 2023), and similar data have been effectively used to study blue whiting distribution in the Barents Sea, Greenland, Portugal, and wider NE Atlantic (Heino et al. 2008, Gonçalves et al. 2017, Post et al. 2019, 2021, Fernandes et al. 2020). Additionally, our models separately accounted for occurrence and abundance, capturing distinct drivers for each. This separation improves reliability by addressing potential biases in trawl catchability, where occurrence reflects habitat suitability, and abundance accounts for relative density variations within suitable areas. However, it is important to note that occurrence models estimate observed presence based on trawl catch data, which may be subject to imperfect detection. As such, zeros in the data may not always represent true absences. As a result, estimated occurrence probabilities may be biased downward, especially in areas or times where detection rates are low. This limitation should be considered when interpreting habitat suitability.

2.3. Covariates

Eight covariates were considered to describe the spatial-temporal patterns in the occurrence, abundance, and length distributions of blue whiting on the Icelandic shelf and slope: (1) Depth (m); (2) bathymetric slope (°); (3) solar time; (4) sea surface temperature (SST; °C); (5) sea bottom temperature (SBT; °C); (6) salinity (psu); (7) chlorophyll ($mg.m^{-3}$); and (8) year. All data extraction, manipulation, processing,

239 exploration, and analyses were performed using R software, version 4.3.0 (R Core
240 Team 2023).
241
242 Depth was calculated as the mean of recordings taken at the start and end of each
243 trawl station. If depth measurements were unavailable, values were extracted using
244 the 'marmap' package (version 1.0.10), which provides gridded bathymetry compiled
245 from observed depth soundings sourced from NOAA's ETOPO1 dataset, combined
246 with spatial interpolation to fill data gaps (Pante & Simon-Bouhet 2013). Bathymetric
247 slope was extracted at the midpoint coordinates of each trawl station using the '*raster*'
248 package (version 3.6-32), which computes slope angles in degrees from elevation
249 differences between raster cells (Hijmans 2023). The 'time of day' was adjusted to
250 local daylight hours using the '*solartime*' package (version 0.0.4) (Wutzler 2021).
251
252 Data for SST, salinity, and SBT were extracted from the Global Ocean Physical
253 Reanalysis (GLORYS12V1) and chlorophyll from the Global Biogeochemical Hindcast
254 (BIORYS2 V4) products, supplied by the Copernicus Marine Environment Monitoring
255 Service (CMEMS), implemented and operated by Mercator Ocean. GLORYS data is
256 a global ocean eddy-resolving reanalysis covering altimetry from 1993 onwards. Data
257 are available as daily or monthly averages distributed on a standard regular grid at
258 1/12° latitude-longitude resolution from the ocean surface to the seafloor (50 depth
259 levels). BIORYS data provides daily or monthly average measurements at a horizontal
260 resolution of 1/4° across 75 vertical depth levels. CMEMS environmental data are
261 designed to provide a realistic representation of environmental and biogeochemical
262 information, validated against in situ observations (Le Traon et al. 2019). These
263 datasets have been widely applied and validated for marine fisheries research (Post

et al. 2021). We utilised monthly mean estimates during the main survey periods (autumn: October; spring: March), aligned with the nearest midpoint coordinates for each trawl station (Figure S1, Figure S2). Monthly means were chosen to reflect the broader environmental context experienced by blue whiting populations during these seasonal periods, considering their potential for movement. This approach also reduces noise from short-term temporal variability around individual trawl dates, providing a more stable characterisation of habitat conditions.

Mean SST, salinity, and chlorophyll were extracted from surface layers (5–50 m) to maximise the reliability of satellite-derived data. Although these surface variables may not precisely represent conditions at the depths where blue whiting were caught, they provide a robust relative index capturing the separate surface currents and water masses at the spatial and temporal resolution of this study. Given the diel vertical migrations of blue whiting, surface conditions are assumed to influence their distribution during at least part of the day.

Explanatory variables were explored for outliers, and the presence of collinearity using plots, Pearson correlation coefficients, and variance inflation factors (VIF) according to standard protocols (Zuur et al. 2010). Continuous explanatory variables were standardised (difference from the mean divided by the corresponding standard deviation) to avoid numerical estimation problems and improve interpretation of the parameters.

2.4. Statistical analysis

2.4.1. Model framework and fitting

We applied hierarchical Bayesian spatial-temporal geostatistical models that account for barriers (Bakka et al. 2019) to estimate and predict the probability of occurrence, mean abundance, and mean length of blue whiting in response to environmental and spatial-temporal predictors (Objective 1). We fitted the models using the integrated nested Laplace approximation (INLA) approach, implemented via the '*R-INLA*' package (version 25.03.24) (Rue et al. 2009, Lindgren & Rue 2015). Independent analyses were undertaken for the spring and autumn fishery surveys. The response variable used to characterise the abundance of blue whiting was continuous, with a high prevalence of zeros (autumn = 14.3% and spring = 53.8%), and high levels of dispersion (i.e. with few outstandingly large catches). Therefore, a 'hurdle' modelling approach was employed, analysing two different response variables to describe the distribution of blue whiting. First, the occurrence (Y_{st}), of blue whiting at location *s* and time *t*, was modelled using a Bernoulli distribution. Second, for positive observations only, the NPUE (Z_{st}) was used as an indicator of conditional-to-presence abundance, modelled using a gamma distribution with a log link. Lastly, we calculated the conditional-to-presence mean length (U_{st}), weighted by the proportional density in each length class of a station, and modelled using a Poisson distribution:

$$Y_{st} \sim Bernoulli(\pi_{st})$$

$$logit(\pi_{st}) = \alpha^{(Y)} + f(x_s) + v_{st}^{(Y)} + \eta_{id(st)}^{(Y)} \quad (1)$$

$$Z_{st} \sim \begin{cases} Gamma(\mu_{st}, k) & if\ Y_{st} = 1 \\ 0 & if\ Y_{st} = 0 \end{cases}$$

$$log(\mu_{st}) = \alpha^{(Z)} + f(x_s) + v_{st}^{(Z)} + \eta_{id(st)}^{(Z)} \quad (2)$$

$$U_{st} \sim \begin{cases} Poisson(\lambda_{st}) \; if \; Y_{st} = 1 \\ 0 \qquad\qquad\qquad if \; Y_{st} = 0 \end{cases}$$

$$log(\lambda_{st}) = \alpha^{(U)} + f(x_s) + v_{st}^{(U)} + \eta_{id(st)}^{(U)} \quad (3)$$

Here, π_{st} represents the probability of occurrence, linked to the linear predictor using a logit link function; μ_{st} denotes the mean NPUE with k as the shape parameter of the Gamma distribution, accounting for extra variation; and λ_{st} represents the mean length. The parameters $\alpha^{(Y)}$, $\alpha^{(Z)}$, $\alpha^{(U)}$ are the model intercepts. Smooth terms $f(x_s)$ were included for explanatory variables using cubic regression splines (cyclic cubic regression splines for solar time), constructed as basis functions using the '*mgcv*' package (version 1.9-1) (Wood 2017). The basis functions form the underlying structure of the smooth curves and were fitted as linear terms in the model (Zuur & Ieno 2018). The number of knots ranged from 4–8, selected through backward selection and capped at a maximum of 10 knots to retain biological interpretability. Smooth terms were applied to the full dataset without an interaction for year, and therefore represent time-invariant effects that reflect average relationships across the study period. Random effects for trawl identity (*id*) are denoted by $\eta_{id(st)}^{(Y)}$, $\eta_{id(st)}^{(Z)}$, and $\eta_{id(st)}^{(U)}$, modelled as independent and identically distributed (iid) effects. The non-stationary spatial-temporal correlated random effects (SRF) for fish occurrence, abundance, and mean length, $v_{st}^{(Y)}$, $v_{st}^{(Z)}$ and $v_{st}^{(U)}$, were modelled using the stochastic partial differential equations (SPDE) approach (Lindgren et al. 2011). The spatial effect was modelled as a continuously indexed Gaussian field, approximated with a Matérn covariance function using a Gaussian Markov random field (GMRF). A Delaunay

triangulation, forming a dense triangular mesh, was constructed on the spatial domain to serve as the structure for representing the field (Figure S3). The mesh was constructed with a minimum vertex gap ('cutoff') of 24 km. A coastline physical barrier was applied, assuming the spatial range (distance at which two data points are effectively independent) was 0.1 of the in-water range (Bakka et al. 2019). This barrier model causes spatial correlation to decay ten times faster with distance across land than water, effectively forcing it to navigate around the barrier. Finally, an outer extension was included in the mesh to avoid a "boundary effect", which can be evident through increased variance at the borders of the mesh (Lindgren & Rue 2015).

We explored persistent, and opportunistic spatial-temporal patterns for each of the six models described above (three models each for spring and autumn surveys), following the terminology of Paradinas et al. (2020). A persistent pattern was modelled using a single spatial effect for all years, with temporal variations captured by an additive temporal trend for year. An opportunistic pattern involved different and uncorrelated spatial effects for each year, along with an additive temporal trend that captures changes in intensity.

Default priors were assigned to all fixed-effect parameters, designed as approximations of non-informative priors to minimize their influence on the posterior distribution. Penalized complexity (PC) priors were applied to the SRF parameters – specifically to the range and marginal standard deviation (Simpson et al. 2017, Fuglstad et al. 2019). These priors provide a principled way to avoid overfitting by shrinking model components toward a predefined base model (e.g. no spatial or temporal structure) unless the data strongly support added complexity. PC priors were

362 defined such that the probability of the spatial range exceeding a specified threshold,
363 and the marginal standard deviation exceeding a specified value, was constrained to
364 small, predefined values (Table 2).
365
366 ***2.4.2. Model selection and validation***
367
368 Models with varying covariates and spatial-temporal effects were compared using
369 stepwise backward selection based on the lowest Deviance Information Criterion (DIC;
370 Spiegelhalter et al. 2002), and the widely applicable information criterion (WAIC;
371 Watanabe 2010). We also employed the sum of the log Conditional Predictive Ordinate
372 (CPO) values, derived through leave-one-out cross-validation, as a measure of model
373 fit, with a higher sum indicating better predictive performance (Gneiting & Raftery
374 2007). Due to strong collinearity among SST, SBT, salinity, and chlorophyll, each of
375 these covariates was first tested independently in simplified models to identify the
376 best-performing variable according to the selection metrics. The variable yielding the
377 best model fit was then included in a full starting model alongside all other relevant
378 environmental and spatial covariates (e.g., depth, slope). From this starting point,
379 backward selection was performed by iteratively removing variables to minimize DIC
380 and WAIC while maximizing CPO. This approach ensured collinearity issues were
381 avoided, and the fixed effects component was optimally specified.
382
383 For model validation, we simulated 1,000 sets of regression parameters from the
384 posterior distribution of the model fit, which were then used to generate predicted
385 values. These predicted values were subsequently used to simulate 1,000
386 corresponding datasets using the '*VGAM*' package (version 1.1-13) (Yee 2023). For

387 the spring and autumn occurrence (Bernoulli distribution) models, we created an
388 average classification table to evaluate model performance in predicting presence-
389 absence relative to the observed data (**Error! Reference source not found.**). For the
390 abundance and length (Gamma distribution) models, average frequency tables were
391 constructed from the simulated datasets for comparison with the observed data
392 (Figure S4). Additionally, the sum of the squared Pearson residuals (dispersion
393 statistic) for the observed data was compared with that of the simulated datasets. We
394 further performed residual diagnostics using the '*DHARMa*' package (version 0.4.7)
395 (Hartig 2022), utilizing the 1,000 simulated fitted values to check for systematic
396 patterns and to confirm the appropriateness of the model fits. This process included
397 plotting residuals against fitted values and versus each covariate in the model. Sample
398 variograms were also constructed to assess spatial-temporal dependency for each
399 model fit.
400
401 ***2.4.3. Spatial-temporal predictions and variability***
402
403 To generate spatial predictions, we constructed a regularly spaced grid with a 10 x 10
404 km resolution across the study area, chosen to balance computational efficiency with
405 the spatial precision needed to capture key environmental and spatial patterns. We
406 retained only grid cells located within 30 km of trawl stations and excluded those falling
407 within the barrier region defined by the spatial mesh. Covariates were estimated for
408 each grid cell as outlined in Section 2.3. To ensure consistency with the fitted model
409 structure, the same spline basis functions used during model fitting were applied to
410 the predictor variables at each grid cell, so that predictions reflected the smooth,
411 nonlinear relationships learned during model training. We then created a projector

matrix using a spatial mesh approach to accurately map grid cell coordinates to model parameters, ensuring the spatial structure of the data were incorporated. To account for model uncertainty and generate predictions, we simulated 1,000 sets of regression parameters from the posterior distribution of the model fit. These parameter sets were used to predict the occurrence, NPUE, and mean length of blue whiting, incorporating both predictor variables and spatial-temporal random effects (accounting for grid cell locations across different years). The final predicted values were obtained by taking the mean of the 1,000 predictions generated for each grid cell for each year.

To address our primary objectives of examining spatial persistence, variability, and temporal trends, as well as their implications for identifying population substructure, we summarized the spatial-temporal predictions following the methodology described by Lindegren et al. (2022). For spatial persistence and variability (Objective 2), we estimated the predicted occurrence, abundance, and length of blue whiting during the spring and autumn by calculating the median and coefficient of variation (CV) for each grid cell across the time series. Prior to analysis, NPUE predictions were log10-transformed to stabilize the variance and mitigate potential biases from hauls with extreme values. For nursery area identification, fish were interpreted as small (<22 cm, immature) or large (≥22 cm, mature) based on the proportion of mature individuals across length classes (Jacobsen et al. 2024).

To investigate spatial variability in temporal trends of occurrence, abundance, and length distributions (Objective 3), we employed two approaches. First, we performed linear regression for each grid cell, using the predicted probability of occurrence, log10-transformed abundance, and mean length as response variables, with year as

437 the predictor. The slope of the regression line was used to assess long-term trends,
438 with positive slopes indicating increases and negative slopes indicating decreases in
439 these metrics over time. Second, we conducted a Principal Component Analysis (PCA)
440 on the covariance matrix of the predicted probabilities of occurrence, log abundance,
441 and mean length. We extracted the first principal component (PC1) loadings to identify
442 regions exhibiting similar long-term trends, revealing potential spatial-temporal
443 patterns in subpopulation distribution.
444
445 ***2.4.4. Detecting population substructure***
446
447 To identify potential subpopulations and delineate spatial patterns in blue whiting
448 distribution (Objective 4), we conducted a clustering analysis using spatial persistence,
449 variability, and temporal variables derived from occurrence, abundance, and length-
450 based models using the 'cluster' package (version 2.1.8) (Maechler et al. 2024). This
451 analysis was performed independently using two approaches: PCA and temporal trend
452 analysis based on slopes from linear regression models (Lindegren et al. 2022).
453
454 To incorporate geographic relationships into the clustering, we calculated pairwise
455 Euclidean distances between grid cell coordinates to create a spatial distance matrix.
456 This matrix captures the relative proximity of grid cells and was integrated into the
457 clustering process to ensure that spatial patterns were appropriately considered.
458
459 The first clustering analysis ('PCA') used variables derived from the median values,
460 coefficients of variation, and the first principal component (PC1) loadings for
461 occurrence, abundance, and mean length. All variables were standardized before

462 calculating the Euclidean distance matrix to ensure equal contributions to the
463 clustering. We then combined this distance matrix with the spatial distance matrix,
464 applying a weight factor of 5% to the spatial component (Lindegren et al. 2022). This
465 was undertaken to prioritize ecological patterns in the clustering process. Hierarchical
466 clustering was performed using Ward's method, which iteratively merges clusters by
467 minimising the total within-cluster variance to create compact groups (Murtagh &
468 Legendre 2014).
469
470 The second clustering analysis ('Linear temporal trend') used variables derived from
471 the median values, coefficients of variation, and the slopes of linear regression models
472 fitted to each grid cell. Following the same procedure, we standardized these variables
473 and calculated the Euclidean distance matrix. The ecological distance matrix was then
474 combined with the spatial distance matrix using the same weighting factor, and
475 hierarchical clustering with Ward's method was applied.
476
477 To determine the optimal number of clusters, we used a combination of dendrogram
478 plotting and silhouette analysis using the '*factoextra*' (version 1.0.7) (Kassambara &
479 Mundt 2020). The silhouette method evaluates how similar each point is to its own
480 cluster compared to other clusters, providing a measure of cluster validity. We
481 calculated silhouette widths for each possible number of clusters to assess cluster
482 cohesion and separation, identifying the optimal number of clusters based on the
483 highest average silhouette width, which indicated the most coherent clustering
484 structure.
485

3. Results

3.1. Model Selection and Seasonality

Models including SST and SBT consistently outperformed those with salinity and chlorophyll across most metrics, with differences exceeding 1% and reaching up to 128% (**Error! Reference source not found.**). Final models included year, time of day, depth, SST, and bathymetric slope, except for the spring length model, where bathymetric slope was excluded due to limited deepwater data. Model selection favoured opportunistic temporal structures for all seasons, highlighting dynamic distribution shifts over time.

Mean (baseline) probability of occurrence, abundance, and length were lower in spring than in autumn. The probability of occurrence in spring (0.11, CI: 0.08–0.14%) was only 11% of that in autumn (0.96, CI: 0.92–0.98). Similarly, baseline abundance in spring (0.070, CI: 0.06–0.08) was 28% of autumn levels (0.25, CI: 0.22–0.29). Estimated length was 12% greater in autumn (28.19 cm, CI: 27.85–28.53 cm) than in spring (25.10 cm, CI: 24.63–25.58 cm).

3.2. Occurrence

Trends in blue whiting occurrence across years were consistent between spring and autumn surveys, with an increase from 1996 to 2003, followed by a decline until 2009 (Figure 2, Figure S5). A strong recovery followed (2009–2014), with subsequent fluctuations. Occurrence was highest at SST >8.0°C (SBT >6.0°C) in autumn, and SST

511 >6.0°C (SBT >4.5°C) in spring (Figure S6). No upper temperature limit was observed,
512 as occurrence continued to rise at the highest recorded SST (9.0–10.0°C) and SBT
513 (8.0–10.0°C). Depth preference ranged from 250–600 m in autumn and 250–500 m in
514 spring, though limited spring sampling beyond 500 m prevented confirmation of an
515 upper depth limit. In autumn, occurrence was highest at intermediate slopes (0.5–
516 1.5°), though slope effects did not show clear patterns during the spring. Occurrence
517 peaked between 20:00 and 05:00 in the spring, with weaker nocturnal trends in
518 autumn.
519
520 The spatial random field (SRF) captured spatial variability unexplained by fixed effects,
521 revealing consistent positive effects (hotspots) along the southern and eastern shelf,
522 and negative effects (depressions) north of Iceland (Figure S7). These patterns
523 showed localised variation over time, including intensified hotspots (e.g. southeast in
524 1996, 2006, 2019), expansions (e.g. to the west in 2013), and strong depressions
525 dissecting the northern shelf (e.g. 2000, 2014, 2016, and 2023). Taking all variables
526 into account, model predictions revealed persistent blue whiting occurrence in
527 southern shelf waters (Median probability > 0.75, CV > 0.5), particularly along the
528 Iceland-Faroe Ridge (IFR), extending over the narrow shelf south of Iceland,
529 southwest over the Reykjanes Ridge, along the west coast of Iceland and towards the
530 East Greenland Shelf (Figure 3A, B). Intermediate occurrence (Median probability =
531 0.25–0.75) was observed on the northern shelf, though with higher variability (CV > 1,
532 Figure S8). Temporal dynamics quantified using PC1 loadings (34.33% of variability)
533 revealed a distinct northwest-to-southeast axis across Iceland (Figure 4A). Temporal
534 dynamics followed different trajectories in these regions, with localized variability.

Linear trends showed no clear regional patterns, instead indicating local-scale variations (Figure 4B).

In spring, the SRF was more fragmented with an absence of clear broadscale patterns, instead characterised by localized hotspots and depressions around the Icelandic shelf (Figure S9). Opportunistic hotspots emerged in the northeast (1998, 2000), the west (2014) and northwest (2022), while a strong depression persisted from 2009 to 2011 in the southeast. Model predictions revealed that occurrence contracted relative to the autumn, yet persistent areas (Probability > 0.75, CV < 1) remained along the southern shelf edge, in particular, the Iceland-Faroes Ridge, southwestern and western shelf (Figure 5A, B). Intermediate occurrence (Median probability = 0.25–0.75) was found on the southern inner shelf and the northern shelf edges, though these fringe areas showed greater annual variability (CV > 1.5; Figure S10). Temporal dynamics captured by the PC1 loadings (52.86%) did not reveal a clear temporal structure across the study area (Figure 6A). However, linear trends showed a general increase in occurrence probability along the IFR, southern, and southwestern shelf (Figure 6B).

3.3. Abundance

Annual blue whiting abundance remained high from 1996 to 2004 before declining until 2009 (Figure 2, Figure S5). A sharp increase followed (2009–2014; +150% in autumn, +200% in spring), stabilizing by 2019. Blue whiting abundance peaked at SST >6°C (SBT > 4.5°C) in spring and >8°C (SBT > 6°C) in autumn. Depth preferences ranged from 250–500 m in spring and 250–600 m in autumn. In autumn, abundance

560 was highest on flat shelf areas (0.2–0.6°) and steep slopes (>2°), while in spring, it
561 showed a weak, but negative relationship with slope. Catchability was highest from
562 20:00 to 05:00 in spring but peaked between 05:00 and 15:00 in autumn.
563
564 During the autumn, broadscale patterns in the SRF revealed hotspots in the south and
565 depressions in the north (Figure S11). Notable localised patterns included an intense
566 hotspot to the west of Iceland in 2013, and a dominant depression in the north which
567 showed strong opportunistic shifts in space, size, and intensity over the study period.
568 Median predicted abundance was highest on the southern Icelandic shelf, particularly
569 along the Iceland-Faroes Ridge and southwestern shelf, where low CV values (CV <
570 1.5) suggested high persistence (Figure 3C, D). The northern shelf supported a stable
571 (CV < 1) but lower-density population. In contrast, the northwest shelf exhibited low
572 median abundance but high variability (CV > 2.5). Similarly, localized areas of low
573 abundance but intermediate variability (CV 1.5–2.5) were evident in shallow waters
574 (<200 m) southeast of Iceland, indicating fluctuating population levels over time
575 (Figure S12). PC1 loadings (41.97%) revealed independent temporal trends in
576 abundance across two broad regions, divided along a northwest-to-southeast axis
577 (Figure 4C). Linear temporal trends identified areas of increasing abundance to the
578 south, west, and north, while declines were seen in the southwest and east (Figure
579 4D).
580
581 In spring, the SRF was more localized (Figure S13), with hotspots recurring over the
582 southwest shelf and southern part of the IFR. A deep depression consistently
583 appeared over the northern extent of the IFR between 2004-2014. Median predictions
584 of high abundance were largely contracted relative to the autumn months,

585 concentrating along the southern, northeastern, and western shelf edges (Figure 5C,
586 D). Lower, variable abundance (CV > 1) was evident in shallow western and
587 southwestern shelf waters, as well as northern waters of the IFR (Figure S14).
588 Temporal dynamics defined according to the PC1 loadings (46.78%) aligned with
589 linear trends (Figure 6C, D). Discrete areas of the southwestern and southeastern
590 shelf showed declining linear abundance, while the northern and eastern shelf
591 exhibited positive trends, particularly over the IFR.
592
593 **3.4. Length**
594
595 Annual trends in blue whiting length reflected shifts in population structure, with
596 smaller individuals dominating in the first five years, followed by a general increase in
597 size until 2007. Median length remained relatively high, with minor declines from
598 2007–2011 and 2019–2023. Larger individuals showed a preference for cooler (2.5–
599 6.0°C in autumn, 1.0–3.0°C in spring; SBT: 1.0–4.0°C), and deeper waters (up to 1000
600 m) of the continental slope (1–2°). Larger individuals were most abundant during
601 daylight hours (06:00–17:00).
602
603 During the autumn, hotspots and troughs in the SRF, were generally broad, of low
604 intensity, and highly opportunistic (Figure S15). Of note was the presence of deep
605 depressions to the northwest (e.g. 2006-2007, 2010, 2013, 2021) and southern waters
606 adjacent to the coast (2004-2006, 2013, 2021), reflecting the occurrence of smaller
607 individuals in these areas that are not explained by the variables. Spatial predictions
608 of median length reflected the dominance of larger individuals (>22 cm) along the outer
609 shelf and slope (Figure 3E, F). Smaller (<22 cm) fish were prominent within inner shelf

610 waters (<200 m) to the south and northwest of Iceland. These inner shelf waters
611 showed higher variability over the study period (CV > 0.15, Figure S16). Large-scale
612 temporal patterns, defined according to the PC1 loadings (44.89%) indicated
613 independent dynamics to the northeast and southwest of Iceland (Figure 4E). Linear
614 temporal trends revealed an increase in median length across the study area,
615 particularly in shallow shelf waters southeast and northwest of Iceland (Figure 4F).
616
617 In spring, the SRF remained highly opportunistic, with hotspots shifting throughout the
618 east (e.g. 1998-2003), west (e.g. 2021), south (e.g. 2004, 2023) and north (e.g. 2013)
619 of the shelf (Figure S17). Broad depressions were prominent across the western and
620 occasionally southern shelf. Predictions of larger fish were concentrated along the IFR
621 and the eastern shelf edge (Figure 5E, F). Smaller blue whiting remained in inner shelf
622 waters, particularly in the south, southwest, and northwest of Iceland. Variability was
623 highest along the southern and western inshore shelf where smaller fish occurred (CV
624 > 0.1, Figure S18). Temporal dynamics depicted through PC1 loadings (50.05%)
625 aligned with linear trends (Figure 6E, F). Length increased across the IFR, the
626 southern and southwestern shelf, remained stable in the north, and declined in the
627 northeast.
628
629 **3.5. Population substructure**
630
631 During the autumn, clustering based on ecological variables revealed four distinct
632 population substructures when temporal dynamics were represented by PC1 loadings
633 (Figure 7A). These included: (1) the southern shelf edge and IFR, where high and
634 persistent occurrence and abundance were observed; (2) a deepwater slope and

northwest shelf region, characterised by persistent low occurrence and abundance, with larger individuals; (3) the west and southern shelf, comprising a localised region with distinct temporal trajectories, variable abundance, and smaller individuals; and (4) the northeast shelf, which exhibited persistent occurrence, low abundance, and distinct temporal dynamics. Slope-based clustering produced three broader clusters in autumn (Figure 7B), including a consolidated southern core group, a distinct western shelf group with variable trajectories, and peripheral low-abundance areas in northern and deeper waters.

In spring, PC1-based clustering resulted in three groupings in which the separation between southern, western, and northern regions were retained (Figure 7C). However, slope-based clustering only showed two main groupings (Figure 7D): a central region of higher occurrence and abundance and outer fringe areas with lower values. Overall, PC1-based clustering captured finer-scale spatial patterns and temporal nuance, while slope-based clustering emphasized broader, directional trends in population dynamics.

4. Discussion

Understanding the environmental and spatial drivers of marine fish distribution is essential for effective fisheries management. This study examines the factors influencing blue whiting distribution in Icelandic waters using Bayesian hierarchical spatial-temporal models. Our results indicate that physical features (depth, bathymetric slope), environmental conditions (SST/SBT), and temporal factors (time of day, year, season) shape blue whiting distribution patterns. Additionally, the spatial

660 random field (SRF) captured localized hotspots and depressions in predicted
661 occurrence, abundance and length, suggesting the influence of unmeasured
662 ecological interactions, oceanographic processes, or migration dynamics. We discuss
663 the role of these drivers in structuring blue whiting populations in Icelandic waters,
664 emphasizing the need to account for both measured and unmeasured processes in
665 species distribution models to improve fisheries management.
666
667 Blue whiting is traditionally considered a mesopelagic species, and the use of
668 demersal bottom trawl survey data introduces potential limitations in interpreting the
669 results. An unknown fraction of blue whiting likely remains higher in the water column
670 and outside the trawl's sampling volume, and this fraction may vary depending on
671 factors such as season, depth, time of day, density, and size (Johnsen & Godø 2007).
672 However, pelagic trawling observations suggest that blue whiting exhibit strong
673 avoidance behaviour toward the bottom, which may increase the effective sampling
674 height of demersal trawl gear (Heino et al. 2008). Additionally, blue whiting, particularly
675 young individuals, are commonly found in shelf areas and regularly caught in bottom
676 trawl surveys, as seen in the Barents Sea, Greenland, and Portugal (Heino et al. 2008,
677 Gonçalves et al. 2017, Post et al. 2019). Further support comes from acoustic
678 recordings from the International Ecosystem Summer Surveys in the Nordic Seas
679 (IESSNS), conducted since 2016, which show that in summer, blue whiting in Icelandic
680 waters is primarily associated with the shelf edge rather than deeper basins, as
681 observed in the Norwegian Sea (Ólafsdóttir et al. 2024). This shelf-based pattern
682 aligns with bottom trawl catch locations in the current study. Taken together, these
683 factors suggest that while bottom trawl surveys may not capture the full extent of blue
684 whiting distribution, they provide a reliable indicator of occurrence and relative

abundance in shelf-associated areas. However, our findings should be interpreted within the known limitations of trawl gear and its variable catchability for benthopelagic species.

Another limitation relates to demographic resolution. While body length served as a proxy for demographic variation in this study, we acknowledge that access to direct age data would provide a more robust framework for testing population-level demographic effects, including age-related habitat use and density dependence. Studies on related pelagic species, such as Atlantic herring, have demonstrated clear age-related differences in habitat use, migration patterns, collective behaviour, and population structure, suggesting similar dynamics may be relevant for blue whiting (Huse et al. 2010, Macdonald et al. 2018, Slotte et al. 2025). Future studies incorporating age-structured information would allow for a more explicit analysis of how intrinsic factors interact with environmental variability to shape blue whiting distribution and habitat use.

4.1. Role of temperature, Depth, and Bathymetry in Population structure

Blue whiting distribution in Icelandic waters is strongly influenced by temperature, depth, and bathymetric features (Figure 2, Figure S5). The species primarily occupies depths of 200–600 m, with SST >6°C in spring and >8°C in autumn (SBT: >4.5°C in spring, >6°C in autumn). These preferences align with observations across the NE Atlantic. For instance, in the Bay of Biscay and Celtic Sea, blue whiting inhabits depths of 100–500 m at temperatures of 9–13°C (Persohn et al. 2009). West of the British Isles, the species occupies shelf waters at 200–550 m and spawns at 9–11°C

(Johnsen & Godø 2007, Miesner & Payne 2018). Egg survival and larval development peak at 6 to 10°C, with an upper thermal limit of ~14.5°C (Coombs & Hiby 1979, Hátún et al. 2009b). Narrow optimal spawning conditions likely facilitate larval ascent to food-rich surface waters, enhancing survival (Miesner & Payne 2018). In Greenland, annual increase in blue whiting abundance coincides with warmer temperatures (>4–6°C) at depths of 250–700 m, conditions that likely increase zooplankton availability and promote early life-stage survival, while supporting adult feeding migrations that occur during the summer (Post et al. 2019, 2021). Similarly, in the Barents Sea, warm Atlantic inflows (>5–6°C) facilitate juvenile transport from the Norwegian Sea, increasing abundance (Heino et al. 2008).

Blue whiting occurrence and abundance exhibits regional structuring, with persistence along the Iceland-Faroe Ridge (IFR), the southern, and the southwestern Icelandic shelf (Cluster 1, 3, Figure 7A-D), and fringe population substructures along the northern shelf (Clusters 2, 4, Figure 7A-D). These patterns align with distinct biogeographic features, particularly the GSR, which acts as both a physical conduit and a barrier for population connectivity. The IFR, as a shelf extension of the GSR, provides a continuous pathway at suitable depths (200–600 m), facilitating seasonal feeding migrations from the core NE Atlantic population during their feeding migration into Icelandic waters. Established migration routes generally follow two primary trajectories: a dominant northeast-ward path toward the Norwegian and Barents Seas (Heino et al. 2008, Hátún et al. 2009a) and a secondary northwest-ward route linking the Faroes, Iceland, and Greenland shelves (Hátún et al. 2009a, Post et al. 2019). Depth and slope along the IFR likely facilitate movement by providing a continuous pathway at suitable depths, while deeper waters offshore and adjacent to the ridge

735 may influence migration patterns by shaping the distribution of prey and
736 oceanographic conditions.
737
738 The GSR also acts as a hydrographic boundary, modulating the inflow of warm, saline
739 North Atlantic water into Icelandic waters while restricting the southward penetration
740 of cold Arctic water from the Nordic Seas (Jónsdóttir et al. 2023a). These contrasting
741 water masses shape distinct subpopulations: the southern shelf aligns with optimal
742 thermal conditions, supporting high blue whiting abundance, while the northern shelf,
743 subject to colder Arctic influence, represents a less favourable fringe habitat with lower
744 densities. The combination of bathymetric structure, warm-water inflows, and the
745 formation of dynamic frontal zones where they interact, sustains productive feeding
746 grounds, potentially enhancing larval retention and survival, akin to Atlantic water-
747 driven recruitment mechanisms in the Barents Sea (Astthorsson et al. 2007, Heino et
748 al. 2008, Trenkel et al. 2015). The persistence of blue whiting across the southern
749 Icelandic shelf highlights its dual role as both a migratory corridor and a key residency
750 zone for feeding and growth.
751
752 The distribution of size classes across depths further reflects habitat structuring.
753 Larger individuals occur at greater depths (up to 1000 m) along the continental slope.
754 In the Bay of Biscay, juveniles occupy shallower depths (100–280 m) than adults (100–
755 500 m), despite interannual variation (Persohn et al. 2009). Similarly, in Greenland,
756 younger individuals occur at 250–500 m, while older fish are found at 300–800 m (Post
757 et al. 2019). Acoustic surveys confirm that blue whiting extend beyond shelf and slope
758 regions, reaching depths of 1000 m, though beyond 550 m, they predominantly occupy
759 the mid-water column (Johnsen & Godø 2007). The apparent decline in abundance at

760 greater depths shown in Icelandic waters may therefore reflect the limitations of
761 demersal trawl gear, underestimating true population size.
762
763 Larger blue whiting in Icelandic waters prefer cooler conditions in autumn (SST: 2.5–
764 6°C; SBT: 1–5°C) and spring (SST: 1–3°C; SBT: 1–5°C), falling below the species'
765 typical thermal range during spawning (Miesner & Payne 2018). This pattern mirrors
766 the Barents Sea, where larger, older individuals extend eastward into colder waters at
767 the range's edge (Heino et al. 2008). This shift may reduce competition during strong
768 recruitment years from the NE Atlantic population, suggesting local adaptations among
769 resident subpopulations (Heino et al. 2008). The depth and temperature preferences
770 of larger individuals suggest greater tolerance for environmental variability, supporting
771 their role as generalist predators (Trenkel et al. 2014).
772
773 **4.2. Unexplained Spatial-Temporal Variation**
774
775 ***4.2.1. Density Dependence***
776
777 Pronounced temporal fluctuations were evident in occurrence and abundance along
778 the margins of persistent areas (Figure 3). The strongest variability occurs along the
779 northwestern and northeastern shelf (Cluster 3, Figure 7A-C; Cluster 4, Figure 7A),
780 reflecting dynamic range contraction and expansion. We hypothesize that one key
781 driver of this variability is density-dependent regulation, influenced by fluctuations in
782 the overall NE Atlantic population. As blue whiting abundance increases beyond
783 competition thresholds in core habitats, we expect spillover into marginal areas, driving
784 range expansion and shifts in distribution. Conversely, when population size declines,

785 the range may contract, leading to a more restricted distribution. This aligns with
786 broader patterns observed in other NE Atlantic pelagic species, where density
787 dependence interacts with environmental variability to shape spatial dynamics. A 30-
788 year review of 19 species found that distributional shifts were driven by thermal habitat
789 suitability and density-dependent area use, with range expansion occurring once
790 density thresholds in core habitats were exceeded (Baudron et al. 2020). A clear
791 example is the westward expansion of mackerel into Icelandic and Greenlandic
792 waters, which has been linked to high densities, increasing temperatures, and
793 competition with other pelagic stocks in the Norwegian Sea (Olafsdottir et al. 2019).
794 For blue whiting, however, density-dependent processes appear to operate differently
795 across life stages. In the Bay of Biscay, juveniles expand into marginal habitats when
796 abundance is high, whereas adults do not (Persohn et al. 2009). This likely reflects the
797 fact that adults already occupy a wide range with broader environmental tolerances,
798 reducing the likelihood of exceeding competitive thresholds in core areas. As a result,
799 range expansion under high densities is primarily observed in juveniles, while adults
800 maintain a more stable, widely distributed range (Persohn et al. 2009). In the Barents
801 Sea, localized range contractions and expansions in the east were attributed to
802 interactions between environmental variability and density dependence (Heino et al.
803 2008), further emphasizing that these factors are interconnected.
804
805 The annual trends in blue whiting occurrence and abundance observed in this study
806 support a similar density-environment interaction, where fluctuations in occurrence,
807 abundance, and size structure correspond to NE Atlantic-wide trends in spawning
808 stock biomass (SSB), recruitment (age 1), and fishing mortality (ICES 2023). Peaks in
809 Icelandic blue whiting numbers in 2003, 2014, and 2023 align with high SSB and

increased recruitment years, while declines in 2009 and 2019 coincide with periods of increased fishing pressure, low SSB, and low recruitment in preceding years. These patterns suggest that recruitment pulses in the NE Atlantic drive a density-dependent expansion into Icelandic waters. A key question remains: do these trends reflect a fully integrated NE Atlantic stock, or do localised subpopulations exist within Icelandic waters? While the dominant influence of the NE Atlantic stock is evident, another possibility is that local Icelandic populations, if present, may be shaped by the same density-dependent mechanisms and environmental drivers observed in the wider NE Atlantic. Similar local contingents have been identified in the Barents Sea, where they remain influenced by broader Atlantic stock dynamics (Heino et al. 2008). In Iceland, our findings suggest that spatial structure varies across both broad (northeast vs. southwest) and localized scales, shaped by a complex interplay of density effects, environmental gradients, and regional habitat suitability. Therefore, the existence of local populations cannot be ruled out.

4.2.2. Early Life Stage Dispersal and connectivity

Nursery areas exhibited strong interannual variability in distribution, likely driven by changes in connectivity with upstream spawning grounds. These patterns suggest that oceanographic-driven dispersal pathways play a key role in linking spawning populations to Icelandic nursery areas. The main blue whiting spawning grounds, located west of the British Isles, shift annually due to large-scale oceanographic processes, particularly the strength of the North Atlantic Subpolar Gyre (SPG) (Hátún et al. 2009b, Miesner & Payne 2018). A weak SPG corresponds with a warm-saline regime, promoting an offshore northward shift in spawning distribution. Conversely, a

strong SPG is associated with a cool-fresh regime, leading to a more southerly spawning distribution along the European continental shelf. These shifts influence larval transport pathways, determining the extent to which eggs and larvae are dispersed into downstream nursery zones (Bartsch & Coombs 1997, Skogen et al. 1999). A northward spawning shift during weak SPG phases likely enhances larval transport to Iceland, increasing connectivity with nursery areas. Conversely, a spawning distribution constrained along the European shelf during a strong SPG phase may lead to greater dispersal into the Norwegian Sea, reducing connectivity with Iceland.

Oceanographic conditions in Icelandic waters not only influence larval transport but also determine the suitability of nursery areas for juvenile survival. The interaction between dispersal pathways and favourable environmental conditions, particularly in the southern Icelandic shelf, may support higher retention and survival rates of blue whiting juveniles. In contrast, periods of a strong SPG and lower temperatures can increase food availability in off-shelf regions south of Iceland (Hátún et al. 2016). Observations show an increase in zooplankton abundance with rising temperatures in blue whiting nursery areas south and west of Greenland (Post et al. 2021). Additionally, results from the current study show a strong positive relationship between temperature, blue whiting occurrence, and abundance in Icelandic waters. These findings suggest a local decoupling of shelf and slope zooplankton production from broader ocean basin dynamics (Post et al. 2021). Interannual variability in nursery area hotspots therefore likely results from a combination of large-scale oceanographic processes governing dispersal, and localized habitat suitability. Future research incorporating larval transport and oceanographic modelling would help clarify the

mechanisms shaping nursery area variability and connectivity with the wider NE Atlantic blue whiting stock.

4.3. Persistence During the Spring

In spring, blue whiting persist along the IFR and the southern and southwestern Icelandic shelf (Figure 5A-D; Cluster 1, 3, Figure 7C-D), though at substantially lower occurrence and abundances than in autumn. Juvenile nursery areas were identified along the western and southwestern shelf. The location, range, and intensity of these hotspots varied inter-annually, reflecting opportunistic patterns. These findings suggest the presence of blue whiting nursery areas along the western and southwestern Icelandic shelf (Figure 5A-F). Here, juvenile fish (<22 cm) persist during the spring while mature individuals return to spawning grounds. Nursery areas have been reported to the east (Age-0, August - September) and southwest (Age-1 and 2, June - September) of Greenland (Post et al. 2019). However, the absence of age-1 and 2 fish in Greenland waters from October to December suggests localized movements into adjacent waters during winter and spring. Ontogenetic spatial patterns observed in other gadoids, along with survey data (Jónsdóttir et al. 2023a), support the interpretation that juvenile blue whiting utilize both Greenland (summer–autumn) and Iceland (winter–spring) as nursery areas. The persistence of juvenile blue whiting in localised nursery areas in Icelandic waters across seasons suggests partial residency during early life stages. However, inter-annual variations in the location and intensity of nursery areas are likely influenced by density dependent factors and oceanographic processes affecting connectivity with upstream spawning grounds (see section 4.2).

Adult blue whiting were also prevalent along the southern and eastern Icelandic shelf during spring (Figure 5). This persistence extends beyond early life stages and may indicate resident subpopulations. A resident subpopulation has been identified in the Barents Sea, where allozyme analyses indicate genetic differentiation (Giæver & Stien 1998, Ryan et al. 2005). While the migration, spawning, and seasonal dynamics of this Barents Sea subpopulation remain unclear, it exhibits a distinct demographic structure and a more eastern distribution than the main NE Atlantic migratory stock (Heino et al. 2008). Genetic studies have not confirmed distinct subpopulation structure in Icelandic waters (Ryan et al. 2005), and genetic studies in Greenland waters are lacking. However, Icelandic genetic samples were primarily collected from the southeastern region during peak feeding migration, where migratory individuals likely dominate (Ryan et al. 2005). Further research should investigate the genetic structure of blue whiting in Greenland waters and in western and northwestern Icelandic waters during spring, when migratory fish have returned to their spawning grounds.

During spring, the location, range, and intensity of adult blue whiting persistence, particularly over the IFR, varied interannually. These shifts represent transitions from near absence to high abundance of larger individuals along the primary pathway connecting the Icelandic shelf to the broader Northeast Atlantic population. This trend appears to align with periods of reduced abundance and subsequent recovery in both Icelandic waters and the broader NE Atlantic (see section 4.2.1). This may reflect the connectivity of adult, migratory individuals with the wider NE Atlantic population. However, the continued occurrence of larger individuals in discrete, low-abundance hotspots over time suggests the potential presence of resident subpopulations. The

possibility of local resident spawning populations of blue whiting in Icelandic waters remains unclear. Spawning fish have not been recorded in Icelandic waters, though maturity data are not collected during Icelandic demersal surveys, particularly in spring when spawning would be expected. Spring temperatures around Iceland are generally cooler than in the main spawning area but remain within the tolerance levels for larval survival (Coombs & Hiby 1979). Although eggs and larvae have been recorded in Icelandic waters, they are considered to be a result of oceanographic dispersal from the spawning areas, and not believed to occur in significant numbers (Sveinbjörnsson 1975, Pointin & Payne 2014, Miesner & Payne 2018).

4.4. Conclusion

This study offers a comprehensive analysis of the spatial and temporal dynamics of blue whiting populations in Icelandic waters, shedding light on key environmental, physical and temporal factors that shape the distribution, abundance, and size structures of this species. The persistence of four to five autumn clusters and the shift to a condensed two-cluster structure in the spring highlight the species' adaptability and connectivity across diverse Icelandic and broader marine habitats in the NE Atlantic. Notably, the presence of distinct seasonal feeding and nursery areas suggests that the Icelandic shelf serves not only as a migration route but as essential habitat that supports critical life stages of blue whiting. These dynamics, aligned with observed trends in the broader NE Atlantic population, suggest a complex interplay between local ecological processes and overarching population movements, indicating Icelandic waters may host a unique mixture of both migratory and potentially resident subpopulations.

935

936 The current study shows that Icelandic waters may host smaller, yet significant,
937 subpopulations that contribute to maintaining the species' biocomplexity, which is vital
938 for understanding the full structure of the population. The genetic diversity within these
939 subpopulations adds to the resilience of the species, particularly in the face of climate
940 change and occasional high fishing pressure. This interpretation ties back to the
941 broader aim of identifying population structures on the edges of the species'
942 distribution, which has important implications for fisheries management, especially in
943 areas historically underestimated for their role in the species' ecology. Further
944 research should prioritise fine-scale investigations into the connectivity between
945 Icelandic nursery areas and broader NE Atlantic spawning grounds, including through
946 seasonal genetic and otolith chemical analyses to distinguish potential resident from
947 migratory subpopulations.

948

949 While this study established a general baseline for environmental influences on blue
950 whiting distribution, the strong year effect observed suggest that the relative
951 importance of covariates may vary across annual to decadal scales. These temporal
952 patterns could reflect shifts in key environmental drivers, potentially linked to changes
953 in subpopulation structure or density-dependent processes. Investigating such
954 variation is another important direction for future work - particularly in the context of
955 climate change - and could help determine whether habitat preferences shift in
956 response to changing population dynamics.

957

Together, these efforts provide a foundation for adaptive, ecosystem-based management strategies that reflect the species' full ecological range and support sustainable fisheries across the NE Atlantic.

Supplementary Material

Supplementary material is available for the online version of the manuscript.

Acknowledgements

We are grateful to the MFRI staff that contributed to data collection during spring and autumn Icelandic groundfish surveys. We thank Mikko Heino and the three anonymous referees for their useful comments. BL was supported by Icelandic Research Fund (RANNIS) Grant 239562-051. The project was also supported by NORA grant number j.nr.510-221.

Data Availability

Data are available upon request from the Marine and Freshwater Research Institute (MFRI) database. The R script used in the analyses will be made available upon reasonable request.

References

Astthorsson OS, Gislason A, Jonsson S (2007) Climate variability and the Icelandic marine ecosystem. Deep Sea Research Part II: Topical Studies in Oceanography 54:2456–2477.

Bachiller E, Skaret G, Nøttestad L, Slotte A (2016) Feeding Ecology of Northeast Atlantic Mackerel, Norwegian Spring-Spawning Herring and Blue Whiting in the Norwegian Sea. PLoS ONE 11:e0149238.

Bailey RS (1982) The Population Biology of Blue Whiting in the North Atlantic. Advances in Marine Biology 19:257–355.

Bakka H, Vanhatalo J, Illian JB, Simpson D, Rue H (2019) Non-stationary Gaussian models with physical barriers. Spatial Statistics 29:268–288.

Bartsch J, Coombs S (1997) A numerical model of the dispersion of blue whiting larvae, *Micromesistius poutassou* (Risso), in the eastern North Atlantic. Fisheries Oceanogr 6:141–154.

Baudron AR, Brunel T, Blanchet M, Hidalgo M, Chust G, Brown EJ, Kleisner KM, Millar C, MacKenzie BR, Nikolioudakis N, Fernandes JA, Fernandes PG (2020) Changing fish distributions challenge the effective management of European fisheries. Ecography 43:494–505.

BIORYS2 V4 (no date) Global Ocean Biogeochemistry Hindcast. E.U. Copernicus Marine Service Information (CMEMS). Marine Data Store (MDS).

Brophy D, King PA (2007) Larval otolith growth histories show evidence of stock structure in Northeast Atlantic blue whiting (*Micromesistius poutassou*). ICES Journal of Marine Science 64:1136–1144.

Cadrin SX, Goethel DR, Berger A, Jardim E (2023) Best practices for defining spatial boundaries and spatial structure in stock assessment. Fisheries Research 262:106650.

Ciannelli L, Fisher J, Skern-Mauritzen M, Hunsicker M, Hidalgo M, Frank K, Bailey K (2013) Theory, consequences and evidence of eroding population spatial structure in harvested marine fishes: a review. Mar Ecol Prog Ser 480:227–243.

Coombs SH, Hiby AR (1979) The development of the eggs and early larvae of blue whiting, *Micromesistius poutassou* and the effect of temperature on development. Journal of Fish Biology 14:111–123.

Dolgov AV, Johannesen E, Heino M, Olsen E (2010) Trophic ecology of blue whiting in the Barents Sea. ICES Journal of Marine Science 67:483–493.

Fernandes JA, Frölicher TL, Rutterford LA, Erauskin-Extramiana M, Cheung WWL (2020) Changes of potential catches for North-East Atlantic small pelagic fisheries under climate change scenarios. Reg Environ Change 20:116.

Fuglstad G-A, Simpson D, Lindgren F, Rue H (2019) Constructing Priors that Penalize the Complexity of Gaussian Random Fields. Journal of the American Statistical Association 114:445–452.

Giæver M, Stien J (1998) Population genetic substructure in blue whiting based on allozyme data. Journal of Fish Biology 52:782–795.

Gjøsæter H, Bogstad B, Tjelmeland S (2009) Ecosystem effects of the three capelin stock collapses in the Barents Sea. Marine Biology Research 5:40–53.

GLORYS12V1 (no date) Global Ocean Physics Reanalysis. E.U. Copernicus Marine Service Information (CMEMS). Marine Data Store (MDS).

Gneiting T, Raftery AE (2007) Strictly Proper Scoring Rules, Prediction, and Estimation. Journal of the American Statistical Association 102:359–378.

Gonçalves P, Ávila De Melo A, Murta AG, Cabral HN (2017) Blue whiting (*Micromesistius poutassou*) sex ratio, size distribution and condition patterns off Portugal. Aquat Living Resour 30:24.

Hartig F (2022) DHARMa: Residual Diagnostics for Hierarchical (Multi-Level / Mixed) Regression Models.

Hátún H, Lohmann K, Matei D, Jungclaus JH, Pacariz S, Bersch M, Gislason A, Ólafsson J, Reid PC (2016) An inflated subpolar gyre blows life toward the northeastern Atlantic. Progress in Oceanography 147:49–66.

Hátún H, Payne MR, Beaugrand G, Reid PC, Sandø AB, Drange H, Hansen B, Jacobsen JA, Bloch D (2009a) Large bio-geographical shifts in the north-eastern Atlantic Ocean: From the subpolar gyre, via plankton, to blue whiting and pilot whales. Progress in Oceanography 80:149–162.

Hátún H, Payne MR, Jacobsen JA (2009b) The North Atlantic subpolar gyre regulates the spawning distribution of blue whiting (*Micromesistius poutassou*). Can J Fish Aquat Sci 66:759–770.

Heino M, Engelhard GH, Godø OR (2008) Migrations and hydrography determine the abundance fluctuations of blue whiting (*Micromesistius poutassou*) in the Barents Sea. Fisheries Oceanography 17:153–163.

Hijmans RJ (2023) Raster: Geographic Data Analysis and Modeling.

Hilborn R, Quinn TP, Schindler DE, Rogers DE (2003) Biocomplexity and fisheries sustainability. Proc Natl Acad Sci USA 100:6564–6568.

ICES (2023) Working Group on Widely Distributed Stocks (WGWIDE). ICES Scientific Reports. 5: 82. 991 pp.

Jacobsen JA, Thomassen JA, Sørensen D, Couperus B, Sakinan S, Winning S, Pasterkamp T, Tijssen D, O'Donnell C, O'Malley M, Mullins E, Høines Å, Sørensen Ø, Meissner T, Tøsdal TG-H, Djønne C, Autón U, Climent SR, Carrera P (2024) International blue whiting spawning stock survey (IBWSS) spring 2024. Marine Institute.

Jakobsdóttir KB, Hjörleifsson E, Björnsson H, Sólmundsson J, Kristinsson K, Bogason V (2023a) Handbók um stofnmælingu botnfiska að haustlagi 2023. Hafrannsóknastofnun.

Jakobsdóttir KB, Hjörleifsson E, Pétursson H, Björnsson H, Sólmundsson J, Kristinsson K, Bogason V (2023b) Stofnmæling botnfiska að haustlagi 2023. Framkvæmd og helstu niðurstöður. Hafrannsóknastofnun.

Johnsen E, Godø OR (2007) Diel variations in acoustic recordings of blue whiting (*Micromesistius poutassou*). ICES Journal of Marine Science 64:1202–1209.

Jónsdóttir IG, Björnsson B, Ragnarsson SÁ, Elvarsson BÞ, Sólmundsson J (2023a) Spatial distributional shifts and associated body condition changes of haddock (*Melanogrammus aeglefinus*) following population expansion. ICES Journal of Marine Science:fsad108.

Jónsdóttir IG, Karlsson H, Björnsson H, Sólmundsson J, Jakobsdóttir KB, Bogason V (2023b) Handbók um stofnmælingu botnfiska á Íslandsmiðum 2023. Hafrannsóknastofnun.

Jónsdóttir IG, Karlsson H, Pétursson H, Björnsson H, Sólmundsson J, Bogason V (2023c) Stofnmæling botnfiska á Íslandsmiðum 2023 - framkvæmd og helstu niðurstöður Icelandic groundfish survey 2023 – implementation and main results. Hafrannsóknastofnun.

Kassambara A, Mundt F (2020) Factoextra: Extract and Visualize the Results of Multivariate Data Analyses.

Kearney B, Hilborn R (2022) Solutions to world-wide fisheries problems are mostly local or regional. ICES Journal of Marine Science 79:997–1004.

1074 Keating JP, Brophy D, Officer RA, Mullins E (2014) Otolith shape analysis of blue whiting
1075 suggests a complex stock structure at their spawning grounds in the Northeast Atlantic.
1076 Fisheries Research 157:1–6.
1077 Kerr LA, Hintzen NT, Cadrin SX, Clausen LW, Dickey-Collas M, Goethel DR, Hatfield EMC,
1078 Kritzer JP, Nash RDM (2017) Lessons learned from practical approaches to reconcile
1079 mismatches between biological population structure and stock units of marine fish.
1080 ICES Journal of Marine Science 74:1708–1722.
1081 Kloppmann M, Mohn C, Bartsch J (2001) The distribution of blue whiting eggs and larvae on
1082 Porcupine Bank in relation to hydrography and currents. Fisheries Research 50:89–109.
1083 Le Traon PY, Reppucci A, Alvarez Fanjul E, Aouf L, Behrens A, Belmonte M, Bentamy A,
1084 Bertino L, Brando VE, Kreiner MB, Benkiran M, Carval T, Ciliberti SA, Claustre H,
1085 Clementi E, Coppini G, Cossarini G, De Alfonso Alonso-Muñoyerro M, Delamarche
1086 A, Dibarboure G, Dinessen F, Drevillon M, Drillet Y, Faugere Y, Fernández V, Fleming
1087 A, Garcia-Hermosa MI, Sotillo MG, Garric G, Gasparin F, Giordan C, Gehlen M,
1088 Gregoire ML, Guinehut S, Hamon M, Harris C, Hernandez F, Hinkler JB, Hoyer J,
1089 Karvonen J, Kay S, King R, Lavergne T, Lemieux-Dudon B, Lima L, Mao C, Martin
1090 MJ, Masina S, Melet A, Buongiorno Nardelli B, Nolan G, Pascual A, Pistoia J, Palazov
1091 A, Piolle JF, Pujol MI, Pequignet AC, Peneva E, Pérez Gómez B, Petit De La Villeon
1092 L, Pinardi N, Pisano A, Pouliquen S, Reid R, Remy E, Santoleri R, Siddorn J, She J,
1093 Staneva J, Stoffelen A, Tonani M, Vandenbulcke L, Von Schuckmann K, Volpe G,
1094 Wettre C, Zacharioudaki A (2019) From Observation to Information and Users: The
1095 Copernicus Marine Service Perspective. Front Mar Sci 6:234.
1096 Lindegren M, van Deurs M, Maureaud A, Thorson JT, Bekkevold D (2022) A spatial statistical
1097 approach for identifying population structuring of marine fish species: European sprat
1098 as a case study. ICES Journal of Marine Science 79:423–434.
1099 Lindgren F, Rue H (2015) Bayesian Spatial Modelling with *R* - INLA. J Stat Soft 63.
1100 Lindgren F, Rue H, Lindström J (2011) An Explicit Link between Gaussian Fields and Gaussian
1101 Markov Random Fields: The Stochastic Partial Differential Equation Approach. Journal
1102 of the Royal Statistical Society Series B: Statistical Methodology 73:423–498.
1103 Logemann K, Ólafsson J, Snorrason Á, Valdimarsson H, Marteinsdóttir G (2013) The
1104 circulation of Icelandic waters – a modelling study. Ocean Sci 9:931–955.
1105 Maechler M, Rousseeuw P, Struyf A, Hubert M, Hornik K (2024) Cluster: Cluster Analysis
1106 Basics and Extensions.
1107 Mahe K, Oudard C, Mille T, Keating J, Gonçalves P, Clausen LW, Petursdottir G, Rasmussen
1108 H, Meland E, Mullins E, Pinnegar JK, Hoines Å, Trenkel VM (2016) Identifying blue
1109 whiting (*Micromesistius poutassou*) stock structure in the Northeast Atlantic by otolith
1110 shape analysis. Can J Fish Aquat Sci 73:1363–1371.
1111 Miesner AK, Payne MR (2018) Oceanographic variability shapes the spawning distribution of
1112 blue whiting (*Micromesistius poutassou*). Fish Oceanogr 27:623–638.
1113 Murtagh F, Legendre P (2014) Ward's Hierarchical Agglomerative Clustering Method: Which
1114 Algorithms Implement Ward's Criterion? J Classif 31:274–295.
1115 Ólafsdóttir AH, Aradóttir SE, Kennedy J, dos Santos Schmidt TC (2024) Results of the
1116 Icelandic part of the International Ecosystem Summer Survey in Nordic Seas (IESSNS)
1117 in July 2023 on R/V Árni Friðriksson. Hafrannsóknastofnun.
1118 Olafsdottir AH, Utne KR, Jacobsen JA, Jansen T, Óskarsson GJ, Nøttestad L, Elvarsson BÞ,
1119 Broms C, Slotte A (2019) Geographical expansion of Northeast Atlantic mackerel
1120 (Scomber scombrus) in the Nordic Seas from 2007 to 2016 was primarily driven by
1121 stock size and constrained by low temperatures. Deep Sea Research Part II: Topical
1122 Studies in Oceanography 159:152–168.

Pálsson ÓK, Bjarnasson H (2011) Long-term changes in trophic patterns of Iceland cod and linkages to main prey stock sizes. ICES Journal of Marine Science 68:1488–1499.

Pampoulie C, Brix S, Randhawa HS (2024) The Greenland–Scotland Ridge in a Changing Ocean: Time to Act? Marine Ecology:e12830.

Pante E, Simon-Bouhet B (2013) Marmap: A Package for Importing, Plotting and Analyzing Bathymetric and Topographic Data in R. PLoS ONE 8:e73051.

Paradinas I, Conesa D, López-Quílez A, Esteban A, Martín López L, Bellido J, Pennino M (2020) Assessing the spatiotemporal persistence of fish distributions: a case study on two red mullet species (*Mullus surmuletus* and *M. barbatus*) in the western Mediterranean. Mar Ecol Prog Ser 644:173–185.

Persohn C, Lorance P, Trenkel VM (2009) Habitat preferences of selected demersal fish species in the Bay of Biscay and Celtic Sea, North-East Atlantic. Fisheries Oceanography 18:268–285.

Pointin F, Payne MR (2014) A Resolution to the Blue Whiting (*Micromesistius poutassou*) Population Paradox? PLoS ONE 9:e106237.

Post S, Fock HO, Jansen T (2019) Blue whiting distribution and migration in Greenland waters. Fisheries Research 212:123–135.

Post S, Werner KM, Núñez-Riboni I, Chafik L, Hátún H, Jansen T (2021) Subpolar gyre and temperature drive boreal fish abundance in Greenland waters. Fish and Fisheries 22:161–174.

R Core Team (2023) R: A Language and Environment for Statistical Computing.

Rue H, Martino S, Chopin N (2009) Approximate Bayesian Inference for Latent Gaussian models by using Integrated Nested Laplace Approximations. Journal of the Royal Statistical Society Series B: Statistical Methodology 71:319–392.

Ryan AW, Mattiangeli V, Mork J (2005) Genetic differentiation of blue whiting (*Micromesistius poutassou* Risso) populations at the extremes of the species range and at the Hebrides–Porcupine Bank spawning grounds. ICES Journal of Marine Science 62:948–955.

Simpson D, Rue H, Riebler A, Martins TG, Sørbye SH (2017) Penalising Model Component Complexity: A Principled, Practical Approach to Constructing Priors. Statistical Science 32:1–28.

Skogen MD, Monstad T, Svendsen E (1999) A possible separation between a northern and a southern stock of the northeast Atlantic blue whiting. Fisheries Research 41:119–131.

Smedbol RK, Stephenson R (2001) The importance of managing within-species diversity in cod and herring fisheries of the north-western Atlantic. Journal of Fish Biology 59:109–128.

Sólmundsson J, Karlsson H, Björnsson H, Jónsdóttir IG, Jakobsdóttir KB, Bogason V (2020) A manual for the Icelandic groundfish survey in spring 2020. HV 2020-08. Marine and Freshwater Research Institute, Reykjavik.

Spiegelhalter DJ, Best NG, Carlin BP, Van Der Linde A (2002) Bayesian Measures of Model Complexity and Fit. Journal of the Royal Statistical Society Series B: Statistical Methodology 64:583–639.

Sveinbjörnsson S (1975) On the accurrence of juvenile blue whiting (*Micromesistius poutassou*) at Iceland. ICES CM 1975/H:39. 8 pp.

Trenkel VM, Huse G, MacKenzie BR, Alvarez P, Arrizabalaga H, Castonguay M, Goñi N, Grégoire F, Hátún H, Jansen T, Jacobsen JA, Lehodey P, Lutcavage M, Mariani P, Melvin GD, Neilson JD, Nøttestad L, Óskarsson GJ, Payne MR, Richardson DE, Senina I, Speirs DC (2014) Comparative ecology of widely distributed pelagic fish species in the North Atlantic: Implications for modelling climate and fisheries impacts. Progress in Oceanography 129:219–243.

1172 Trenkel VM, Lorance P, Fässler SMM, Høines ÅS (2015) Effects of density dependence,
1173 zooplankton and temperature on blue whiting *Micromesistius poutassou* growth. J Fish
1174 Biol 87:1019–1030.
1175 Walker ND, Maxwell DL, Le Quesne WJF, Jennings S (2017) Estimating efficiency of survey
1176 and commercial trawl gears from comparisons of catch-ratios. ICES Journal of Marine
1177 Science 74:1448–1457.
1178 Was A, Gosling E, McCrann K, Mork J (2008) Evidence for population structuring of blue
1179 whiting (*Micromesistius poutassou*) in the Northeast Atlantic. ICES Journal of Marine
1180 Science 65:216–225.
1181 Watanabe S (2010) Asymptotic Equivalence of Bayes Cross Validation and Widely Applicable
1182 Information Criterion in Singular Learning Theory. Journal of Machine Learning
1183 Research 11:3571–3594.
1184 Wood SN (2017) Generalized Additive Models: An Introduction with R (2nd edition).
1185 Chapman and Hall/CRC.
1186 Wutzler T (2021) Solartime: Utilities Dealing with Solar Time Such as Sun Position and Time
1187 of Sunrise.
1188 Yee TW (2023) VGAM: Vector Generalized Linear and Additive Models.
1189 Zuur AF, Ieno EN (2018) GAM and zero-inflated models. Highland Statistics Ltd, Newburgh,
1190 United Kingdom.
1191 Zuur AF, Ieno EN, Elphick CS (2010) A protocol for data exploration to avoid common
1192 statistical problems: *Data exploration*. Methods in Ecology and Evolution 1:3–14.
1193

1194 Table 1: Details of response and explanatory variables included in the model framework.

Covariate type	Predictor	Description	Reference
Model	Season	The season (spring / autumn) that sampling took place.	(Jakobsdóttir et al. 2023a b, Jónsdóttir et al. 2023b c)
Response	Occurrence	The occurrence (0/1) of blue whiting in the trawl.	(Jakobsdóttir et al. 2023a b, Jónsdóttir et al. 2023b c)
	Abundance	Total catch quantity (number) of blue whiting scaled by the swept area of the trawl (number.cm.trawl^{-1}).	
	Length	The length class by cm group from the sampled catch.	
Survey	ID	The unique trawl station.	(Jakobsdóttir et al. 2023a b, Jónsdóttir et al. 2023b c)
	Trawl location	Longitude (X utm) and latitude (Y utm) coordinates of the mid trawl position.	
	Year	The numerical year of sampling (1996 - 2023).	
Environmental	Sea surface temperature (SST)	Monthly mean (°C) at a 0.083 x 0.083° spatial resolution.	CMEMS, (GLORYS12V1)
	Sea bottom temperature (SBT)	Monthly mean (°C) at a 0.083 x 0.083° spatial resolution.	CMEMS, (GLORYS12V1)
	Salinity (Sal)	Monthly mean (10^3) at a 0.083 x 0.083° spatial resolution.	CMEMS, (GLORYS12V1)
	Chlorophyll (Chl)	Monthly mean (mg/m^3) at a 0.25 x 0.25° spatial resolution.	CMEMS, (BIORYS2 V4)
	Depth (m)	Sea floor depth (m). Observation, or calculated using the '*marmap'* and '*raster*' packages.	(Pante & Simon-Bouhet 2013, Hijmans 2023)
	Bathymetric slope (Slope)	Gradient (°) of the sea floor calculated from the '*raster*' package	(Hijmans 2023)
	Solar time	Solar time at the mid-point of a trawl station adjusted to local daylight hours using the 'solartime' package.	(Wutzler 2021)

1195

1196 Table 2: Penalised complexity prior parameters for the spatial random field in each
1197 submodel, defined as the threshold range and standard deviation values beyond which
1198 the prior probability was constrained.

Season	Model	Range	Prob	Sd	Prob
Spring	Occurrence	55	<0.0001	3.5	<0.0001
	Abundance	35	<0.0001	2	<0.0001
	Length	55	<0.0001	1	<0.1
Autumn	Occurrence	55	<0.0001	3	<0.0001
	Abundance	35	<0.05	3	<0.05
	Length	50	<0.0001	1	0.1

1199

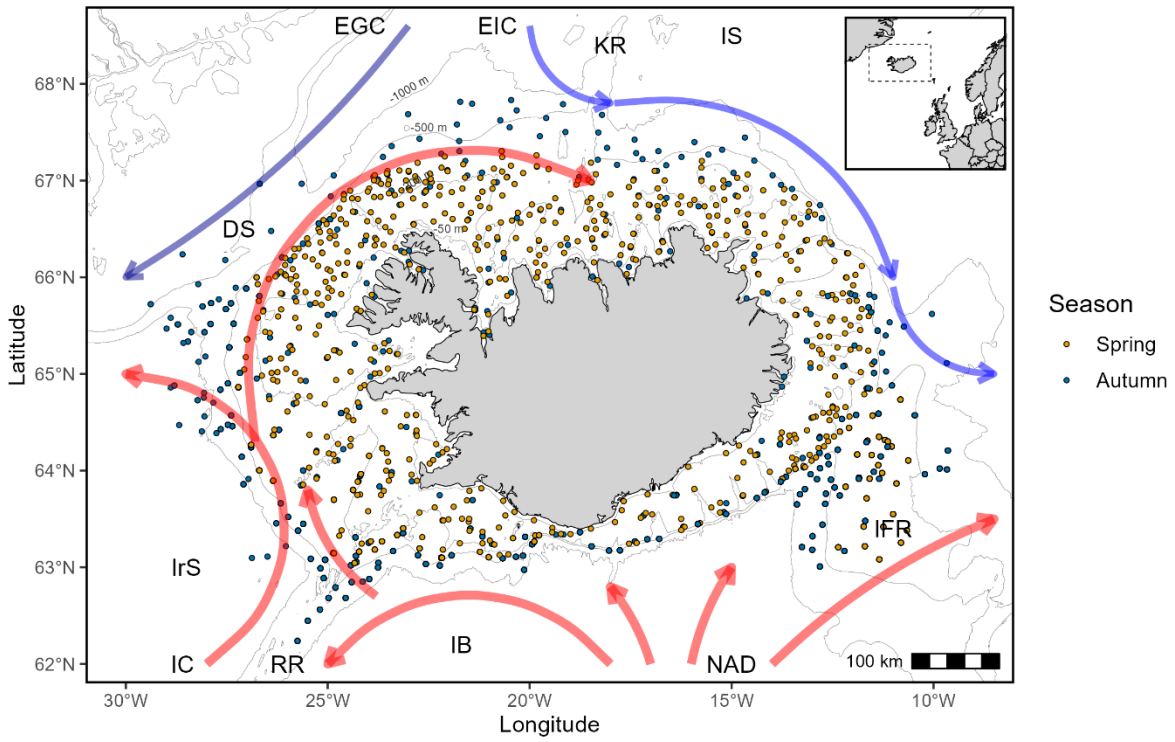

Figure 1: Map of sampling stations from the 2023 annual spring (late February to early April) and autumn (mid-September to early November) groundfish surveys, highlighting key oceanographic currents and topographic features. The red (warm) and blue (cool) arrows indicate the relative temperatures and directions of the prevailing currents. Abbreviations: **DS** (Denmark Strait), **EGC** (East Greenland Current), **EIC** (East Iceland Current), **IB** (Iceland Basin), **IC** (Irminger Current), **IFR** (Iceland-Faroe Ridge), **IrS** (Irminger Sea), **IS** (Iceland Sea), **KR** (Kolbeinsey Ridge), **NAD** (North Atlantic Drift), **RR** (Reykjanes Ridge).

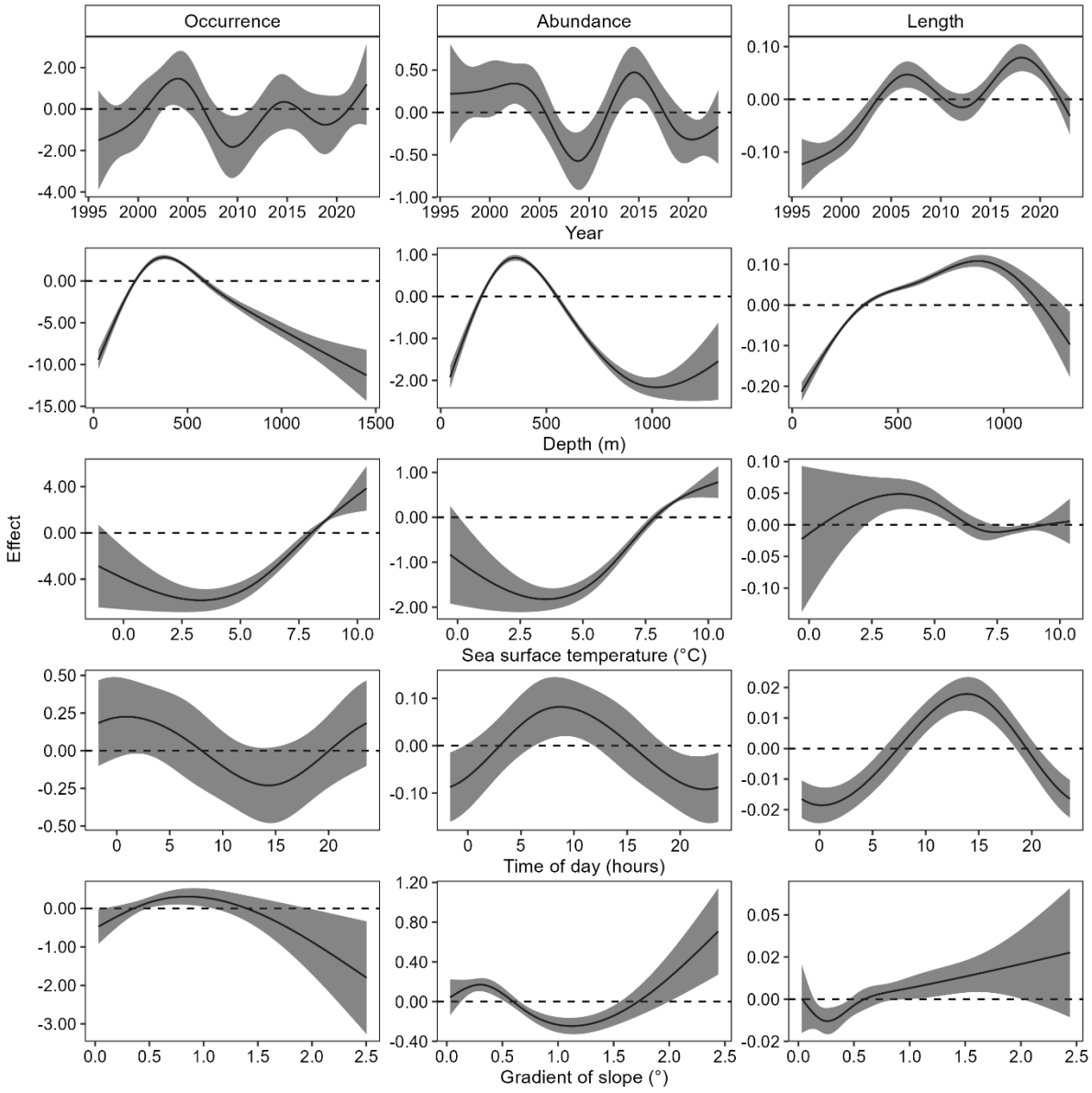

Figure 2: Estimated effect of year, time of day (hrs), depth (m), sea surface temperature (°C), and bathymetric slope covariates on the probability of occurrence, abundance and mean length of blue whiting during the autumn months (late September to early November) from 1996 to 2023 around the Iceland shelf and slope. The estimated effect is presented as smooth functions with grey shaded areas representing the 95% credible intervals.

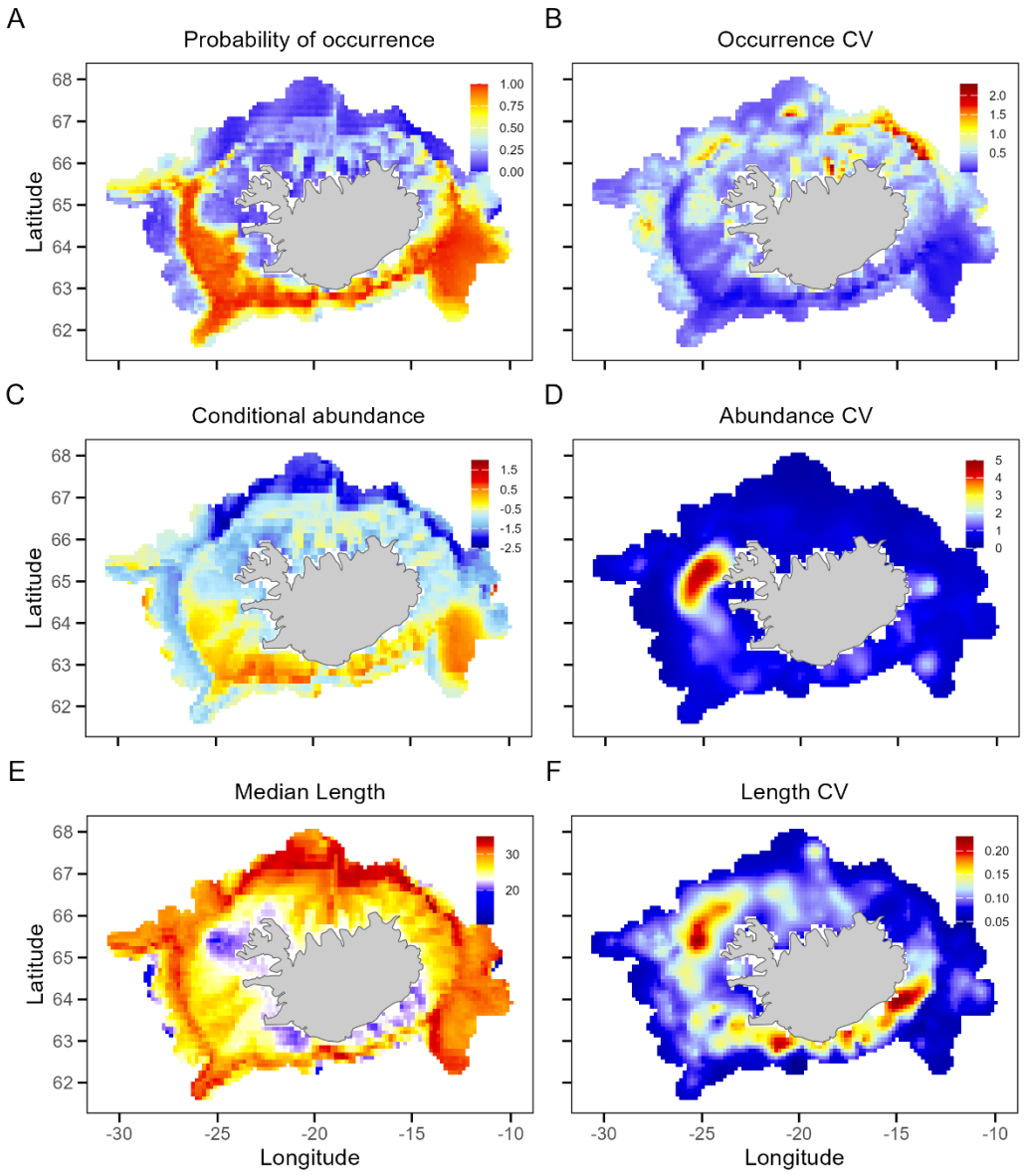

Figure 3: Spatial persistence represented as the median and coefficient of variation for predicted (A-B) occurrence, (C-D) log-transformed abundance, and (E-F) length of blue whiting during the autumn months (late September to early November) from 1996 to 2023, across 10 x 10 km grid cells.

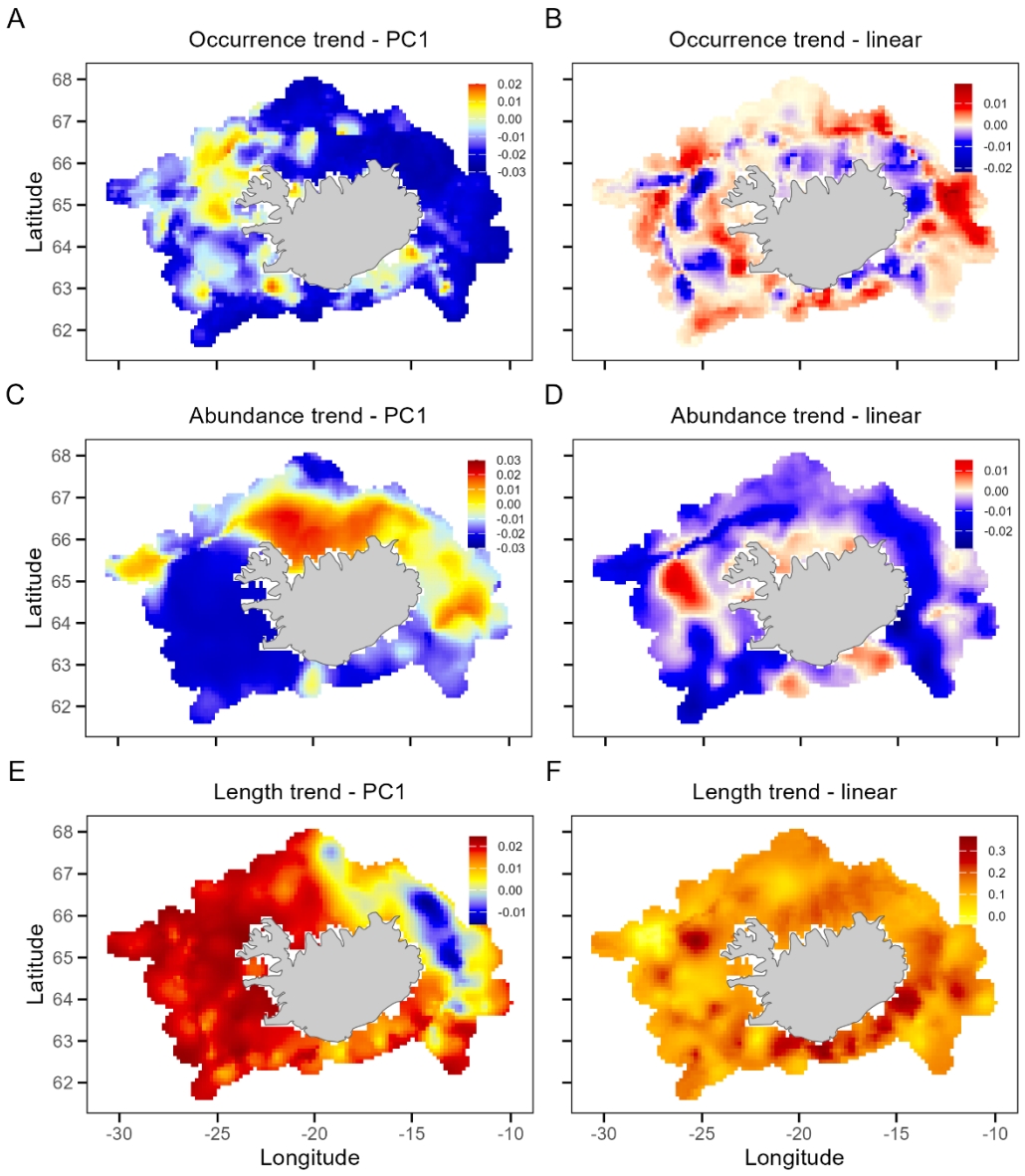

Figure 4: Temporal dynamics of blue whiting during autumn (late September to early November) from 1996 to 2023, represented by loadings on the first principal component (PC1, left column) or linear slopes (right column) of predicted (A-B) occurrence, (C-D) log-transformed abundance, and (E-F) weighted mean length trajectories across 10 x 10 km grid cells.

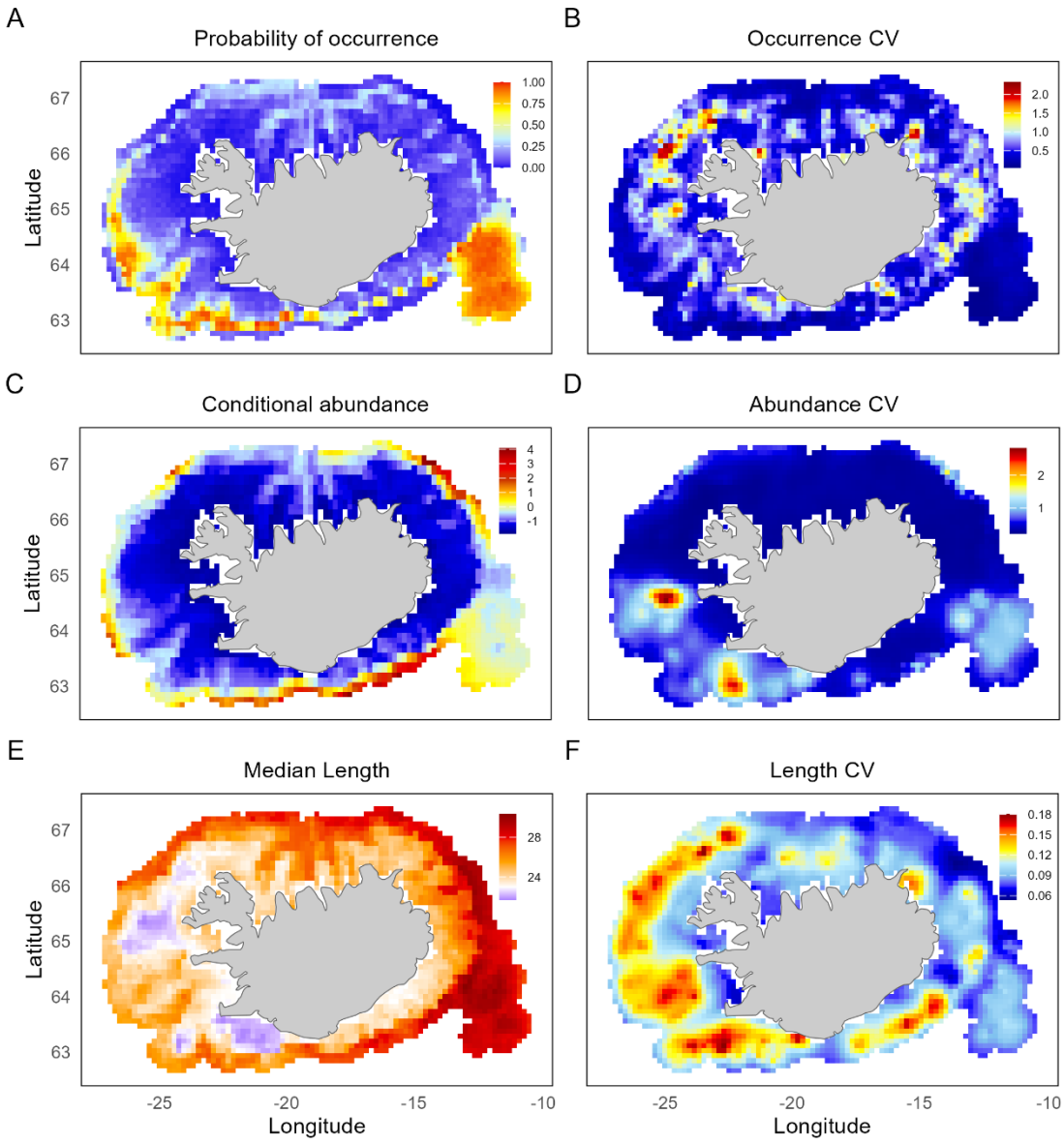

Figure 5: Spatial persistence represented as the median and coefficient of variation for predicted (A-B) occurrence, (C-D) log-transformed conditional abundance, and (E-F) median length of blue whiting during the spring months (late February to early April) from 1996 to 2023, across 10 x 10 km grid cells.

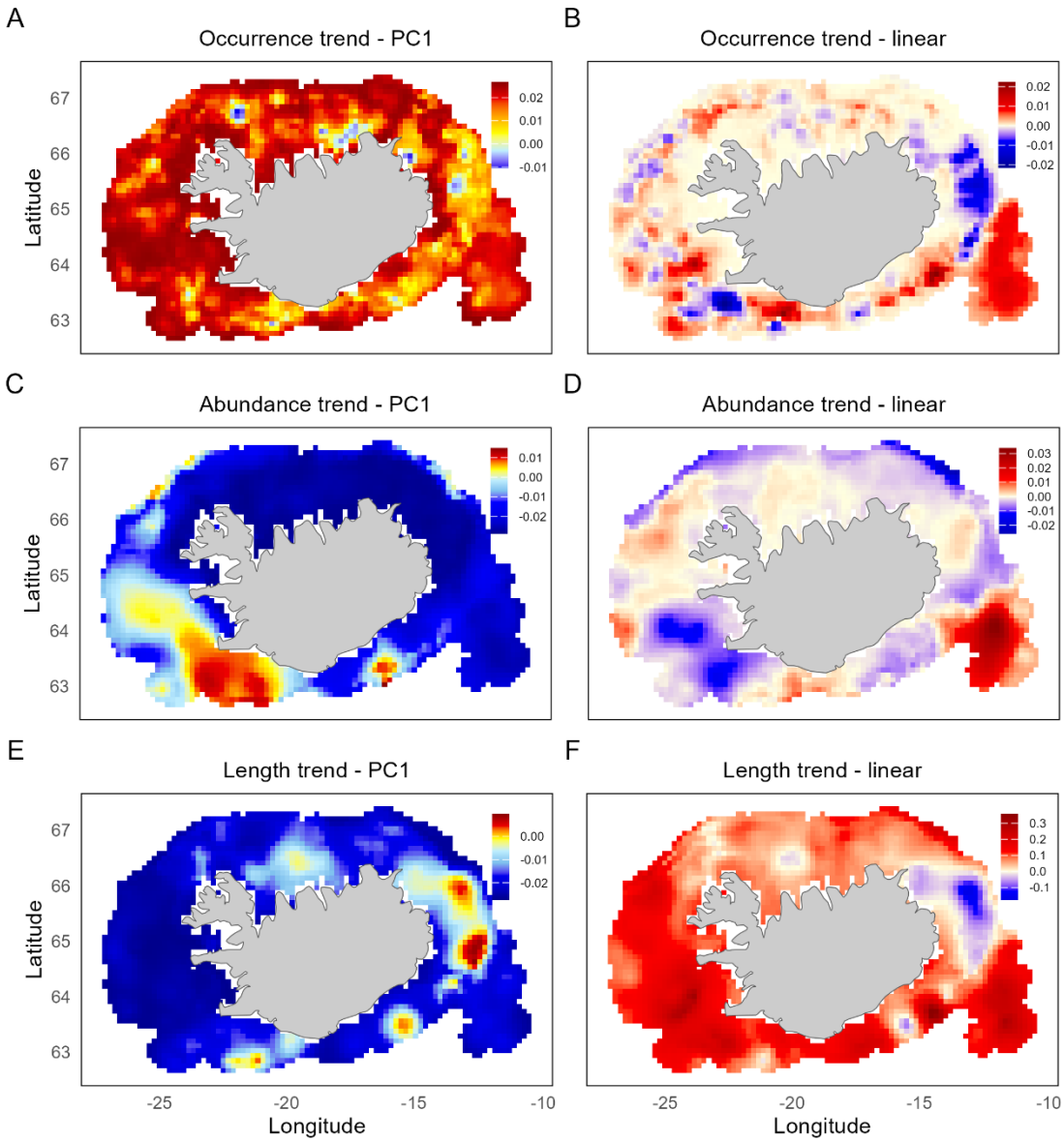

Figure 6: Temporal dynamics of blue whiting during spring months (late February to early April) from 1996 to 2023, represented by loadings on the first principal component (PC1, left column) or linear slopes (right column) of predicted (A-B) occurrence, (C-D) log-transformed abundance, and (E-F) weighted mean length trajectories across 10 x 10 km grid cells.

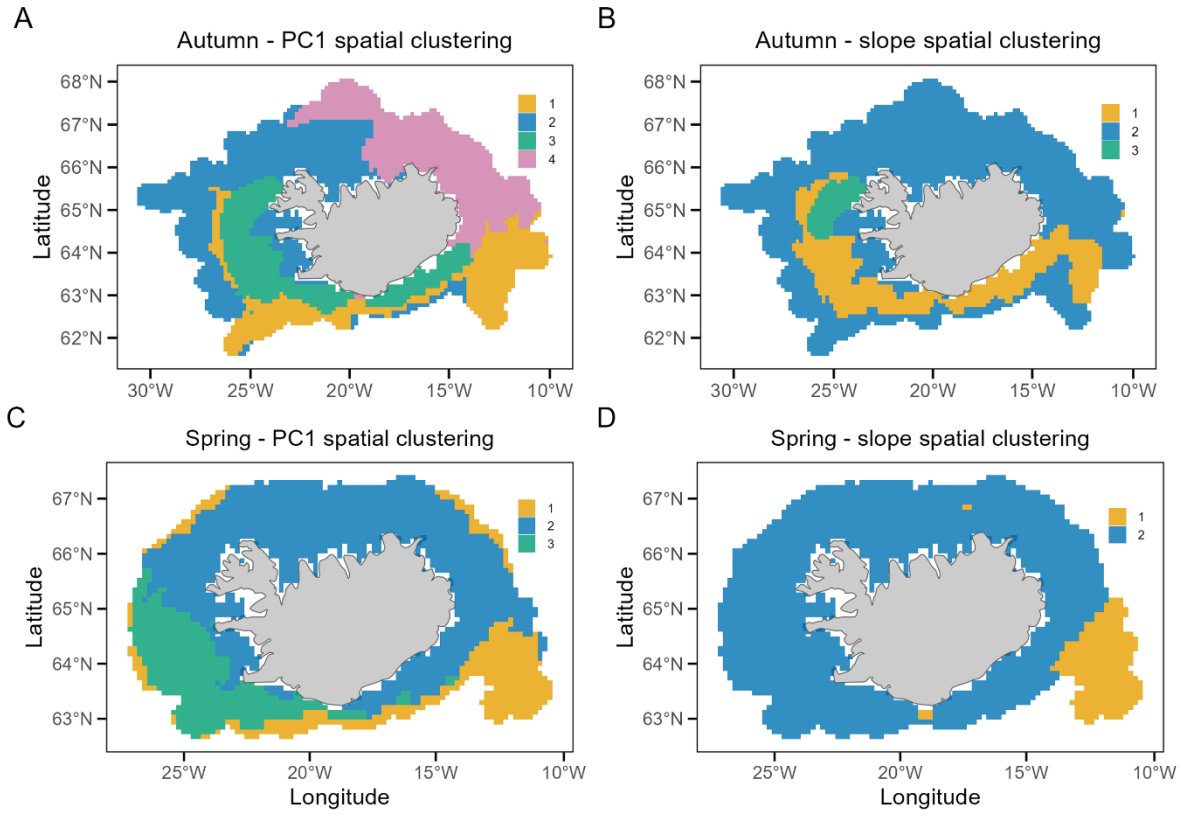

Figure 7: Hierarchical clustering results showing potential population structuring of blue whiting during autumn (A-B, late September to early November) and spring (C-D, late February to early April) from 1996 to 2023. Clustering is based on the median and coefficient of variation of occurrence, abundance, and weighted mean length. Temporal dynamics are represented by either (A, C) the loadings on the first principal component (PC1) or (B, D) the linear slopes of occurrence, abundance and length trajectories by (10 x 10 km) grid cell.